However, the role of oxidized wild-type and FALS-linked mutant SOD1s on these diseases remains unclear.

Human SOD1 has four cysteine residues, Cys^6, Cys^{57}, Cys^{111}, and Cys^{146}. An internal disulfide bond exists between Cys^{57} and Cys^{146} (14, 15), which contributes to the high stability of the SOD1 protein. This disulfide bond is highly conserved in SOD1s from various organisms, including yeast, plants, flies, fishes, and mammals. In contrast, two free cysteines, Cys^6 and Cys^{111}, are not conserved. Actually, yeast, fungi, and spinach (plants) have no free cysteines, and residue 6 is Ala and residue 111 is Ser in these organisms (16). More evolved organisms, such as flies, fishes, and mammals, including the Japanese monkey, have only one free cysteine, Cys^6. Only humans and great apes (chimpanzee and orangutan) have two free cysteines, Cys^6 and Cys^{111} (17). Notably, the amino acid sequence of chimpanzee SOD1 is identical to that of human SOD1. Although the evolutionary process may differ from humans and great apes, chicken SOD1 has three free cysteines, including Cys^6 and Cys^{111}. The third free Cys residue is located at the C terminus, Cys^{154} (18). Because free cysteines are generally reactive, and wild-type SOD1 is less thermo-stable than Ser^{111}-SOD1 or Ala^6-SOD1 (19), the A6C and S111C mutations during evolution are puzzling. In particular, Cys^{111} is located at the surface of the SOD1 molecule and is thought to be highly reactive. De Beus *et al.* (20) reported that Cys^{111} was modified with persulfide (S-SH) in a human SOD1 isolated from erythrocytes that is commercially available (Sigma). The persulfide SOD1 was more resistant to copper-induced aggregation than wild-type SOD1 (20). The sulfur atom of cysteine is able to assume several different oxidation states. Reversible oxidation of cysteine to disulfide (-S-S-) or sufenic acid (-SOH) is readily accomplished by thiols, such as DTT, 2-ME, glutathione, or thioredoxin. In contrast, oxidation to sulfinic acid ($-SO_2H$) or sulfonic acid ($-SO_3H$) is not reduced by these thiols under physiological conditions (21). For example, one cysteine in the active site of peroxiredoxin (Prx) is oxidized to sulfinic acid ($-SO_2H$) by incubation with an excess of substrate of this enzyme, H_2O_2, and rereduced by a specific enzyme, sulfiredoxin, but not by general thiols (22, 23).

An upper shifted band of human wild-type or mutant SOD1s, with the exception of mutant C111S, on SDS-PAGE has been observed under a variety of conditions: during purification (24) or when hydrogen peroxide or copper ion is added (see Fig. 1). The SOD1 in the upper band is speculated to be irreversibly linked to another molecule via a covalent bond at Cys^{111}; however, neither the molecule nor the modification site have been identified. Ube Industries Ltd. developed recombinant human SOD1 chemically modified with 2-mercaptoethanol at Cys^{111} (2-ME-SOD1; Cys^{111}-S-S-CH_2CH_2OH). This 2-ME-SOD1 is stable for many years in aqueous solution, showing neither degradation nor a loss of activity. Thus, in this study, the role of Cys^{111} in oxidative damage of human SOD1 was investigated by comparing 2-ME-SOD1 and wild-type SOD1, and the identity of the molecule that is bound to human SOD1 in the upper band on SDS-PAGE was explored. Through mass spectrometry and limited proteolysis, it was determined that the mass size of the molecule is 32 and 48 and that the modification site in SOD1 is Cys^{111}. We demonstrated that Cys^{111} in human SOD1 is selectively oxidized to cysteine sulfinic acid (Cys-SO_2H) and to cysteine sulfonic acid (Cys-SO_3H) even by air oxidation. Moreover, a polyclonal antibody was raised against a synthesized peptide containing Cys^{111}-SO_3H. This antibody, denoted as anti-C111ox-SOD1, reacted with the upper band (oxidized SOD1) but not the original band by Western blot analysis. Using this anti-C111ox-SOD1, the role of Cys^{111} on the generation of SOD1 charge isomers and the presence of oxidized SOD1 in the spinal cord of ALS mice were investigated.

EXPERIMENTAL PROCEDURES

Materials—All chemicals used in this study were obtained either from Wako Pure Chemical Industries Ltd. (Osaka, Japan), Nacalai Tesque, Inc. (Kyoto, Japan), or Sigma unless specified otherwise. Recombinant human SOD1, chemically modified with 2-mercaptoethanol (2-ME-SOD1), was kindly provided from Ube Industries Ltd. Horseradish peroxidase-conjugated goat anti-rabbit IgG and horseradish peroxidase-conjugated rabbit anti-goat IgG were purchased from Dako (Denmark). Lysylendopeptidase (Achromobacter Proteinase I) was obtained from Wako Pure Chemical Industries Ltd. (Osaka, Japan). Sequencing grade modified trypsin was purchased from Promega (Madison, WI). Sinapinic acid and α-cyano-4-hydroxycinnamic acid for matrix of MALDI-TOF MS were obtained from Bruker Daltonik GmbH (Bremen, Germany).

Conversion of 2-ME-SOD1 to Wild-type SOD1—2-ME-SOD1 was incubated with 20 mM 2-ME for 1 h on ice and desalted with a PD-10 column. The resultant wild-type SOD1 and 2-ME-SOD1 were used in the experiments with the exception of the experiments in Fig. 1, *B* and *C*.

Production and Purification of Wild-type and Mutant SOD1 Proteins—Overproduction of SOD1s by the baculovirus/insect cells system and purification of SOD1 proteins were carried out as described previously (25).

Oxidation of SOD1 and the Analyses with MonoQ Column—For strong oxidation, SOD1s diluted with miliQ water (1 mg/ml) were incubated with 5 mM H_2O_2 for 1 h at room temperature. For mild air oxidation, SOD1s diluted with miliQ water or appropriate buffer were filtered with a 0.22-μm filter (Millipore) and were slowly stirred at 30 rpm with a rotator (rotator RT-50; Taitec). The buffer or water containing oxidized SOD1s was changed with buffer A (2 mM potassium phosphate, pH 7.4) on a PD-10 column (Amersham Biosciences). The SOD1s were applied to a high performance liquid chromatograph (AKTA Explorer 10S) at a flow rate of 1 ml/min on a MonoQ column (MonoQ™ 4.6/100 PE; Amersham Biosciences). After washing with buffer A, the bound proteins were eluted with a linear gradient of KCl (0–100 mM) in buffer A. Adhesive proteins were washed with 0.5 M KCl in buffer A.

Lysylendopeptidase Treatment and Peptide Analyses—SOD1 proteins were reduced with DTT, and the free sulfhydryls were carbamidemethylated by adding iodoacetamide (IA) in the dark at room temperature for 30 min. After desalting on a PD-10 column with 50 mM Tris-HCl (pH 8.8), the proteins were digested with 0.25% (w/w) lysylendopeptidase (Wako Pure Chemicals) at 37 °C for 16 h. The resultant peptides were applied to a reverse-phase high performance liquid chromato-

graph (AKTA Explorer 10S) at a flow rate of 1 ml/min on TSK-GEL ODS-80TM (4.6 × 250 mm; Tosoh). The peptides were separated by two linear gradients of 0–30% acetonitrile for 4 column volumes and 30–40% acetonitrile for 8 column volumes containing 0.05% trifluoroacetic acid. Peptides were detected by their absorbance at 215 nm. The peaks were subjected to the following MS analyses.

MALDI-TOF MS Analysis—MALDI-TOF MS spectra of peptides and proteins were measured on an Ultraflex TOF/TOF mass spectrometer and analyzed by the Flexcontrol 1.2 software package (Bruker Daltonics GmbH, Bremen, Germany). For analyses of peptides, ions generated by a pulsed UV laser beam (nitrogen laser; λ = 337 nm, 5 Hz) were accelerated to a kinetic energy of 20 kV in reflector mode using positive polarity. Metastable ions generated by laser-induced decomposition of the selected precursor ions were analyzed without any additional collision gas. α-Cyano-4-hydroxycinnamic acid (5 mg/ml in 50% acetonitrile containing 0.1% trifluoroacetic acid) was used as a matrix for peptide analyses. For analyses of proteins, the determinations were performed in linear mode using positive polarity. Sinapinic acid (10 mg/ml in 50% acetonitrile containing 0.1% trifluoroacetic acid) was used as matrix for protein analyses. Peptide or protein samples (1 μl each) were mixed with matrix solution (4 μl each), and an aliquot (1 μl each) was applied to a polished stainless steel target (Bruker Daltonics). The mixture was dried in air at room temperature for several minutes.

Infusion ESI MS Analysis for Peptide Sequence—ESI mass spectra were measured on a Bruker Esquire HCT equipped with a quadrupole ion trap (Bruker Daltonics GmbH, Bremen, Germany). The solutions containing peptides digested with lysylendopeptidase were continuously introduced through the electrospray interface with a syringe infusion pump (Cole-Parmer, Vernon Hills, IL) at a flow rate of 5 μl/min. The MS conditions were as follows: nebulizer gas (N_2), 10 p.s.i.; dry gas (N_2), 4 liters/min; dry temperature, 250 °C; capillary voltage, 3500 V; high voltage end plate offset, −500 V; capillary exit, 190.6 V; skimmer, 40 V; trap drive, 166.7. MS/MS spectra were sequenced using BioTool 2.2 software and Sequence editor 2.2 (algorithm provided by Bruker).

Trypsin Digestion for MALDI-TOF MS—SOD1 proteins in 50 mM NH_4HCO_3 were digested with trypsin at 37 °C for 16 h. An aliquot of the digests (10 μl) was boiled, applied to ZipTip C18 P10 (Millipore, Bedford, MA; according to the manufacturer's protocol) for desalting, and then subjected to MALDI-TOF MS analysis. When alkylation is needed, SOD1 proteins in 50 mM NH_4HCO_3 were treated with excess IA in the dark at room temperature for 30 min before trypsin digestion.

In-gel Digestion of Coomassie Brilliant Blue-stained Polyacrylamide Gel for MALDI-TOF MS—The gel bands containing SOD1 protein after SDS-PAGE were clipped out and cut into small pieces in a 1.5-ml microtube. To remove Coomassie Brilliant Blue dye, the chopped gels were washed three times with 50 mM NH_4HCO_3 in 30% acetonitrile by shaking at room temperature for 20 min. The gels were further incubated with 500 μl of acetonitrile at room temperature for 10 min. After removing acetonitrile, the gels were incubated with an alkylating solution (500 μl) consisting of 40 mM IA, 10 mM EDTA, and 50 mM NH_4HCO_3 in the dark at room temperature for 30 min. After washing twice with 50 mM NH_4HCO_3 (500 μl) for 10 min, the gels were incubated with 0.4 μg of trypsin in 50 mM NH_4HCO_3 at 37 °C overnight. After removing the pieces of gels, the remained solution was concentrated with a SpeedVac concentrator and subjected to MALDI-TOF MS analyses.

Preparation of Antibody for Cys^{111}-sulfonylated SOD1—Keyhole limpet hemocyanin-coupled peptide (residues 103–114) containing sulfonylated Cys^{111} (Cys^{111}-SO_3H) was obtained from Sigma. After the initial injection with the peptide-hemocyanin conjugate (200 μg of peptide) mixed with complete Freund's adjuvant, rabbits were subjected to five booster injections, each of 200 μg of peptide with incomplete Freund's adjuvant, administered (at multiple subcutaneous sites) at 1–2-week intervals. Antisera were collected 1 week after the sixth booster injection, and the IgG fraction was precipitated with 50% (w/v) ammonium sulfate. The IgG fraction passed from the wild-type SOD1 coupled to *N*-hydroxysucinimide-activated Sepharose was bound to the oxidized SOD1 coupled to *N*-hydroxysucinimide-activated Sepharose. The bound IgG was eluted with 3 M $MgCl_2$ and collected. The IgG was desalted with a PD-10 column and stored with 0.1 mg/ml bovine serum albumin (BSA) at deep freeze until use. This antibody was denoted as anti-C111ox-SOD1.

SDS-PAGE and Western Blot Analysis—Proteins were subjected to SDS-PAGE (14% gel) and then transferred to a PVDF membrane under semidry conditions by means of a Trans-blot (Bio-Rad). After blocking by incubation with 5% skim milk in Tris-buffered saline (TBS; 20 mM Tris-HCl, pH 8.0, 0.15 M NaCl) for 2 h at room temperature, the membrane was incubated with anti-C111ox-SOD1 (diluted 1:1000), or a goat polyclonal antibody against full-length human SOD1 (25), anti-SOD1 (diluted 1:1000), in TBS containing 0.05% Tween 20 (TBS-T) and 1% skim milk for 2 h at room temperature or for 18 h at 4 °C. After washing with TBS-T, the membrane was incubated with horseradish peroxidase-conjugated anti-rabbit IgG (diluted 1:5000) for anti-C111ox-SOD1 or horseradish peroxidase-conjugated anti-goat IgG (diluted 1:5000) in TBS-T containing 1% skim milk for anti-SOD1, respectively, for 2 h at room temperature. After washing, the chemiluminescence method using an ECL or an ECL plus kit (GE Healthcare) was employed to detect peroxidase activity.

Two-dimensional Gel Electrophoresis—Sample proteins were dissolved in 8 M urea, 2% (w/v) CHAPS, 0.5% (v/v) immobilized pH gradient (IPG) buffer (GE Healthcare), and 12 μl/ml DeStreak™ reagent (GE Healthcare), which forms stable disulfide bonds and prevents nonspecific Cys residue oxidation during isoelectric focusing (26). The samples were applied to 11-cm IPG strips (pH 4–7), and the strips were then isoelectrically focused on an IPGphor isoelectric focusing system (GE Healthcare) according to the following schedule: 500 V-h at 500 V for step and hold, 800 V-h at 1000 V for gradient, 8800 V-h at 6000 V for gradient, and 4000 V-h at 6000 V for step and hold. The strips were equilibrated for 20 min in 50 mM Tris-HCl (pH 8.8) containing 6 M urea, 2% (w/v) SDS, 30% (v/v) glycerol, and 1% (w/v) DTT. Second dimension separation was run on 14% SDS-polyacrylamide gels and followed by Western blot analysis. pI values of spots were calculated according to the graph

showing pH as function of distance at 20 °C and 8 M urea of IPG strips (pH 4–7) provided by the GE Healthcare on-line system.

ELISA—Wild-type SOD1 was air-oxidized, treated with and without 100 mM IA, and then diluted to 500 ng/ml with phosphate-buffered saline (PBS). 100 μl of the samples were added to each well of 96-well microplates (Maxisorp; Nunc), incubated overnight at 4 °C, washed three times with TBS-T, and then blocked for 2 h at room temperature with 1% BSA in PBS. The plates were then washed three times with TBS-T, and 100 μl of anti-C111ox-SOD1 and anti-SOD1 antibodies (diluted 1:1000 in TBS-T) was added, followed by incubation for 1 h at room temperature. The plates were washed three times with TBS-T, and 100 μl of horseradish peroxidase-conjugated anti-rabbit IgG (diluted 1:5000 in TBS-T) for anti-C111ox-SOD1 or horseradish peroxidase-conjugated anti-goat IgG (diluted 1:5000 in TBS-T) for anti-SOD1, respectively, was added and incubated for 1 h at room temperature. After washing five times with TBS-T, the plates were developed using 100 μl of *o*-phenylenediamine dihydrochloride solution, and the reaction was stopped with 25 μl of 2 M HCl. The absorbance of each well was determined at 490 nm with a SPECTRAmax PLUS384 (Molecular Devices).

Animals and Animal Tissue Preparation—Four transgenic mice carrying a high copy number of the human G93A SOD1 gene (B6SJL-TgN[SOD1-G93A]1Gur, G1H-G93A) mice, were purchased from the Jackson Laboratory (Bar Harbor, ME). Two age-matched littermates were used as controls. All animals were handled in accordance with the guidelines for care and use (Tottori University). All four G1H-G93A mice at 110 days of age neurologically exhibited hind limb paralysis, and two littermate mice at 110 days of age did not show any clinical symptoms. The G1H-G93A and littermate mice were euthanized at 110 days of age. Animals were deeply anesthetized with sodium pentobarbital (0.1 ml/100 g of body weight). After perfusion of three G1H-G93A and two littermate mice via the aorta with PBS at 37 °C, they were fixed by perfusion with 4% paraformaldehyde in 0.1 M cacodylate buffer (pH 7.3). The spinal cords were removed and then postfixed in the same solution. The spinal cord of one mouse for Western blot analysis was removed after perfusion with PBS, quickly frozen in liquid nitrogen, and stored at −80 °C until use.

Protein Extraction from G1H-G93A Mouse Spinal Cord—The G1H-G93A spinal cord was homogenized in ice-cold homogenization buffer, 20 mM Tris-HCl (pH 6.8) containing Complete™ miniprotease inhibitor mixture (Roche Applied Science), and 100 mM IA for preventing the secondary oxidation of SH groups. The sample was centrifuged at 17,000 × *g* at 4 °C for 30 min, and the pellet was homogenized in the ice-cold homogenization buffer containing 1% Triton X-100. The sample was centrifuged at 17,000 × *g* at 4 °C for 30 min, the pellet was further homogenized in the ice-cold homogenization buffer containing 1% Triton X-100 and 2% SDS, and the sample was centrifuged at 17,000 × *g* at 4 °C for 30 min. The supernatants of each homogenization, buffer-soluble, Triton X-100-soluble, and SDS-soluble fractions, were subjected to SDS-PAGE and Western blot analyses.

Immunohistochemical Analysis—After fixation, the specimens were embedded in paraffin, cut into 5-μm-thick sections, and examined for immunohistochemical analysis. Sections were deparaffinized and then washed in PBS. Normal serum homologous with the secondary antibody diluted in 1% BSA-containing PBS (BSA-PBS) was used as a blocking reagent. Tissue sections were incubated with anti-C111ox-SOD1 (diluted 1:1000 in BSA-PBS) at 4 °C for 18 h. Bound antibody was visualized by the avidin-biotin-immunoperoxidase complex (ABC) method using the appropriate Vectastain Elite ABC rabbit IgG kit (Vector Laboratories) and 3,3′-diaminobenzidine tetrahydrochloride (Wako, Osaka, Japan) as a chromogen. The endogenous peroxidase activity was quenched by incubation for 30 min with 3% H_2O_2 after the secondary antibody treatment to prevent nonspecific oxidation before anti-C111ox-SOD1 treatment.

SOD1 Activity—SOD1 activity was assayed using the xanthine-xanthine oxidase/cytochrome *c* system as described previously (27).

Protein Assay—SOD1 protein concentrations were estimated using a dimeric molar extinction at 280 nm of 10,800 M^{-1} cm^{-1} (28). Protein concentrations of crude samples were determined using a BCA™ protein assay kit (Pierce) with BSA as a standard.

RESULTS

2-ME-SOD1 Obtained from Ube Industries Ltd. Was Modified with 2-ME Only at Cys^{111}—First, the chemical modification with 2-mercaptoethanol of recombinant human Cu/Zn-SOD (2-ME-SOD1) was confirmed. The molecular mass of 2-ME-SOD1 was determined to be 15,865.5 (supplemental Fig. S1*A*) to 15,871 *m/z* (supplemental Fig. S2*A*), which suggested the presence of 2-ME (76 Da) in apo-human SOD1 (monoisotopic mass, 15,794.86; average mass, 15,804.55). The metals, copper and zinc, of SOD1 were removed during MALDI-TOF MS analysis. Since this recombinant human SOD1 was expressed in *Escherichia coli*, the N terminus was not acetylated. To demonstrate that the 2-ME-SOD1 was in fact modified with 2-ME only at Cys^{111}, the 2-ME-SOD1 was digested with trypsin and then analyzed by MALDI-TOF MS and MS/MS. The mass of the tryptic peptide (2533 *m/z*) indicating residues Asp^{92}–Arg^{115} (2457 *m/z*) plus the mass of 2-ME (76 Da) (supplemental Fig. S1*B*) was analyzed by the collision-induced MS/MS. As shown in supplemental Fig. S1*C*, the major fragment ions, y4 (457.1 *m/z*), y5 (635.9 *m/z*), y6 (772.9 *m/z*), y14 (1530.9 *m/z*), y19 (2074.4 *m/z*), and y23 (2418.7 *m/z*), indicated the presence of 2-ME at Cys111. The mass of the tryptic peptide (933 *m/z*, missed cleavages = 1), residues Ala^1–Lys^9, indicated that another free cysteine, Cys^6, was not modified with 2-ME (supplemental Fig. S1*B*). MS/MS analyses of the residues Ala^1-Lys^9 also indicated that 2-ME was not contained in this peptide (supplemental Fig. S1*D*). These results demonstrated that Cys^{111}, but not Cys^6, was modified with 2-ME. The commercial human SOD1 from Sigma, modified with persulfide (S-SH) or with trisulfide (-S-S-S-) intersubunit linkage at Cys^{111}, exhibits an absorbance peak at 325 nm (20, 29). However, 2-ME-SOD1 did not exhibit the 325 nm peak (data not shown).

Additional 2-ME Treatment Recovered the 2-ME-SOD1 to Wild-type SOD1—Next, the ability to remove 2-ME from Cys^{111} was examined. 2-ME-SOD1 was incubated with 0 (H_2O), 2, 20, and 200 mM 2-ME for 1 h on ice; the excess 2-ME was removed on a PD-10 column with miliQ water, and then the mass of the proteins was analyzed. As shown in supplemental Fig. S2*A*, the incubation with more than 20 mM 2-ME decreased the mass of the protein (from 15,871 to 15,795 *m/z*). The difference in the mass was 76 m/z, indicating that incubation with 20 mM 2-ME removes 2-ME from Cys^{111}. Thus, to confirm this finding, the 2-ME-treated SOD1s were digested with trypsin after incubation with IA, and the mass of the resulting peptides was determined. Removal of 2-ME from Cys^{111}, would allow the SH group of Cys^{111} to be carbamidemethylated by IA, yielding a mass of 2514 (2456 plus 58) *m/z*. As shown in supplemental Fig. S2*B*, the mass of the tryptic peptide containing Cys^{111} (residues Asp^{92}–Arg^{115}) treated with more than 20 mM 2-ME was 2514 *m/z*. In contrast, the mass of the 2-ME-SOD1 treated with H_2O was 2533 *m/z*, indicating that the SH group of Cys^{111} remained bound to 2-ME. These results show that incubation of 2-ME-SOD1 with 2-ME in excess of 20 mM removed 2-ME from Cys^{111}, converting 2-ME-SOD1 to wild-type SOD1. The SOD activities of 2-ME-SOD1 and the wild-type SOD1 were 4181 and 4056 units/mg, respectively, indicating that both SOD1s have similar activities.

Upper Band of Oxidized Human SOD1 on SDS-PAGE Involves Cys^{111}—2-ME-SOD1 and wild-type SOD1 were incubated with various concentrations of H_2O_2 for 20 min and then subjected to reducing SDS-PAGE. Although 2-ME-SOD1 was slightly affected by H_2O_2 treatment, wild-type SOD1 showed an additional upper band when incubated with more than 1 mM H_2O_2 (Fig. 1*A*). When commercial gradient gels (5–20%, e-PAGEL; Atto) were used for the SDS-PAGE, the upper band was not observed (data not shown). It is thought that the two bands are unable to separate on the gradient gels. Next, various purified wild-type and mutant human SOD1 proteins expressed in the baculovirus/insect cell system (25) were oxidized with 1 mM H_2O_2, followed by reducing SDS-PAGE and Western blotting. As shown in Fig. 1*B*, the additional upper band appeared in all SOD1s, except C111S, after oxidation. Furthermore, the effects of various metal ions on the generation of the upper band were investigated. Only the Cu^{2+} ion, among all metal ions examined, formed an upper band similar to that observed after oxidation with H_2O_2 (Fig. 1*C*). Although Fe^{3+} and Fe^{2+} are thought to be oxidants, neither Fe^{3+} (data not shown) nor Fe^{2+} treatment generated the upper band. Next, wild-type SOD1 diluted with various pH buffers was slowly stirred (30 rpm with a rotator) for 24 h at room temperature. As shown in Fig. 1*D*, the upper band was generated when the pH of the incubation buffer was higher than pH 7. These results indicated that Cys^{111} was readily oxidized by oxygen in ambient air and that the sulfhydryl group (SH) of Cys^{111} was needed to provide a thiolate anion (S^-) for the oxidative modification.

Role of Cys^{111} in the Generation of Negatively Charged Molecules after Oxidation—To examine the role of Cys^{111} in the generation of negatively charged molecules after oxidation, 2-ME-SOD1 and wild-type SOD1 were incubated with 5 mM H_2O_2 for 1 h and were applied to a MonoQ column. Some of the

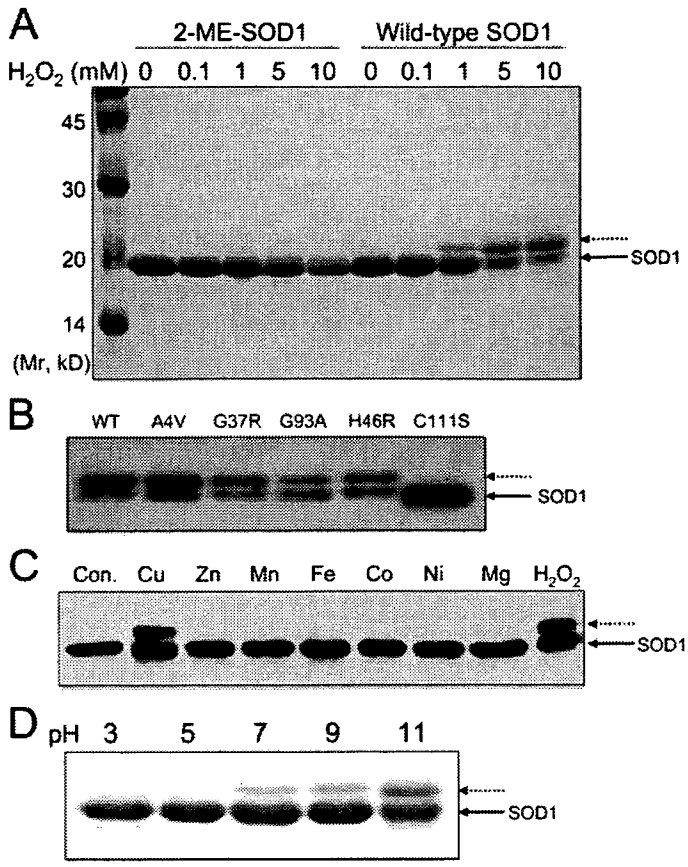

FIGURE 1. **Generation of upper shifted band of SOD1 on SDS-PAGE under reducing conditions.** *A*, 2-ME-SOD1 and wild-type SOD1 treated with various concentrations of H_2O_2 for 20 min, diluted with miliQ water, and boiled with SDS-PAGE loading buffer containing 5% 2-ME. 5 μg of protein/lane was subjected to SDS-PAGE (14% gel). Rainbow™ colored protein molecular weight markers purchased from GE Healthcare were used as molecular weight markers (*left*). *B*, Western blot analyses of wild-type and mutant SOD1s treated with 1 mM H_2O_2 for 20 min. *C*, Western blot analyses of wild-type SOD1 treated with 1 mM $CuCl_2$, $ZnCl_2$, $MnCl_2$, $FeCl_2$, $CoCl_2$, $NiSO_4$, $MgCl_2$, and H_2O_2 for 1 h. Wild-type and mutant SOD1s used in *B* and *C* were produced by the baculovirus/insect cells system. SOD1 proteins in *B* and *C* were immunostained with anti-SOD1. *D*, SDS-PAGE of wild-type SOD1 stirred for 24 h in various pH buffers (50 mM), citric acid-NaOH (pH 3.0), sodium citrate-disodium phosphate-NaOH (pH 5.0), sodium phosphate (pH 7.0), and glycine-NaOH (pH 9.0 and 11.0). The *arrowheads* with *solid lines* indicate SOD1 subunits, and *arrowheads* with *broken lines* indicate modified SOD1 subunits.

fractions were then subjected to reducing SDS-PAGE and Western blotting. Since incubation with 5 mM H_2O_2 caused oxidation of almost all histidine and cysteine residues in bovine SOD1 (3), it is thought that negatively charged molecules were generated in both SOD1s. As shown in the *upper panels* of Fig. 2, *A* and *B*, several peaks containing oxidized SOD1 proteins were eluted with similar patterns in both SOD1s. However, the results of Western blotting were quite different (*lower panels* in Fig. 2, *A* and *B*). In oxidized 2-ME-SOD1, only one fragment (labeled with an *asterisk*) from the first peak and slight polymer bands from the last fractions, which were obtained by washing the column with 0.5 M KCl, were observed (Fig. 2*A*). The single fragment resulting from oxidation of 2-ME-SOD1 has been identified by Ookawara *et al.* (5) as a large fragment cleaved between Pro^{62} and His^{63}. Because Ookawara *et al.* (5) also used recombinant human SOD1 (2-ME-SOD1) obtained from Ube Industries Ltd., it can be concluded that the identity of the single fragment in the present study and that of Ookawara *et al.* (5)

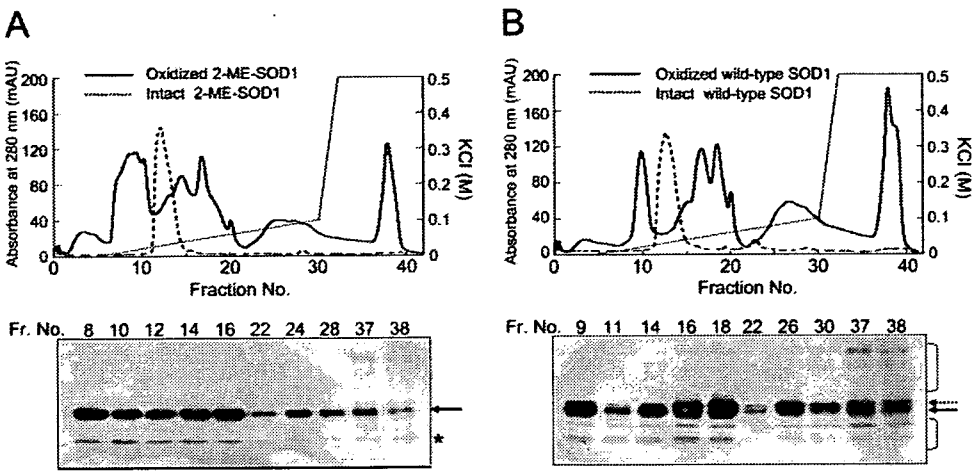

FIGURE 2. **Separation of oxidized SOD1s with a MonoQ column.** 2-ME-SOD1 and wild-type SOD1 were incubated with 5 mM H_2O_2 for 1 h and were applied to a MonoQ column; some fractions were subjected to reducing SDS-PAGE and Western blot analyses. *A*, chromatogram profiles of oxidized and intact 2-ME-SOD1 separated with MonoQ column (*top*), and Western blot analysis of some fractions indicated (*bottom*). *B*, chromatogram profiles of oxidized and intact wild-type SOD1 separated with MonoQ column (*top*), and Western blot analysis of some fractions indicated (*bottom*). SOD1 proteins in *A* and *B* were immunostained with anti-SOD1. The *arrowheads* with *solid lines* indicate SOD1 subunits, and *arrowheads* with *broken lines* indicate modified SOD1 subunits. *mAU*, milliabsorbance units.

are the same. In contrast, oxidation of the wild-type SOD1 resulted in not only the upper band but also in several additional fragments and polymer bands (Fig. 2*B*). Oxidation of Cys^{111} may become a trigger of fragmentation and polymerization. Zhang *et al.* (8) reported that a covalently cross-linked dimer (polymer) of human SOD1 was induced by bicarbonate and H_2O_2. Therefore, the effects of bicarbonate on the oxidation of 2-ME-SOD1 and wild-type SOD1 were investigated. However, no difference in dimer formation between the two SOD1 variants was observed (data not shown), suggesting that the cross-linkage between monomers was not mediated by Cys^{111}.

Identification of the Molecule in the Upper Band—Next, the identity of the molecule in the upper band was explored. Slow stirring in miliQ water did not cause fragmentation and polymerization of SOD1 but generated the upper band. Thus, in order to exclude effects of the buffer system, 2-ME-SOD1 and wild-type SOD1 were oxidized by stirring in miliQ water. Then the molecular masses were measured by MALDI-TOF MS. The air-oxidized wild-type SOD1 showed two masses, 15,792 and 15,838 *m/z*, but the mass of 2-ME-SOD1 did not change (Fig. 3*A*). Fig. 3*B* shows the elusion patterns of air-oxidized 2-ME-SOD1 and wild-type SOD1 on the MonoQ column. The stirred wild-type SOD1 (*solid line*) was separated into two peaks (*a* and *b*), whereas the stirred 2-ME-SOD1 (*dotted line*) was not separated. MALDI-TOF MS also showed that the SOD1 protein in peak *b* also gave two masses, 15,793 and 15,841 *m/z* (Fig. 3*C*), and gave two bands on reducing SDS-PAGE (Fig. 3*D*). It is noteworthy that the SOD activity in peak *b* (3716 units/mg) was similar to the activity in peak *a* (3753 units/mg) and that SOD1 proteins in both peaks retained more than 90% of SOD activity compared with the original wild-type SOD1. These results suggested that oxidative modification at Cys^{111} did not affect on SOD activity and that His residues in the active site were still intact. The difference in mass units between the SOD1 subunit in the upper band and the SOD1 subunit in the original band appeared to be about 48, suggesting the presence of three oxygens at Cys^{111}. Next, the upper and original bands from reducing SDS-PAGE (Fig. 3*D*) of peak *b* from the MonoQ column were clipped out, alkylated with IA, and digested with trypsin. The resultant peptides were subjected to MALDI-TOF MS analyses. In the *upper band*, a major mass, 2505 *m/z*, corresponding to tryptic peptide 92–115 (2457 *m/z*) plus 48 was detected. A minor mass, 2489 *m/z*, corresponding to tryptic peptide 92–115 plus 32 was also observed (Fig. 3*E*). In contrast, in the original band, a mass of 2514 *m/z* resulting from carbamidemethylation (plus 58) of tryptic peptide 92–115 was detected (Fig. 3*F*). These results indicate that amino acids in residues 92–115, probably Cys^{111}, in the upper band, were oxidized with two or three molecules of oxygen (Cys^{111}-SO_2H or Cys^{111}-SO_3H). However, the amounts of these peptides were too small for MS/MS analyses to determine the amino acid sequence.

To obtain greater quantities of oxidized peptides, SOD1 proteins in peaks *a* and *b* separated with the MonoQ column (Fig. 3*B*) were reduced by DTT, alkylated with IA, and digested with lysylendopeptidase, but not with trypsin. The resultant peptides were applied to a reverse-phase high performance liquid chromatograph (ODS column). As shown in Fig. 4*A*, the HPLC elution profiles were nearly identical, but two additional peaks (*d* and *e*) were observed after the last peak (*c*) only in digests from peak *b* of the MonoQ column (*i.e.* the *lower panel*). Peak *c* has already been identified as residues 92–122 containing carbamidemethylated Cys^{111} in previous work (25). When fractions containing the additional peaks *d* and *e* were reapplied to the ODS column, four fractions containing three distinct peaks were obtained (Fig. 4*B*). Each fraction was subjected to MALDI-TOF MS analyses. As a result, peptide *c* in fractions 1 and 2 corresponded to residues 92–122 containing carbamidemethylated Cys^{111} (3320.5 *m/z*), as expected. Peptide *d*, in fractions 2 and 3, and peptide *e*, in fractions 3 and 4, gave masses corresponding to residues 92–122 plus 32 (3295.5 *m/z*) and residues 92–122 plus 48 (3311.6 *m/z*), respectively (Fig. 4*C*).

To directly demonstrate the formation of Cys^{111}-SO_2H and Cys^{111}-SO_3H, these peptides (*c*–*e*), were further analyzed by infusion ESI MS/MS. This method was used to ascertain the site of oxidative modification of SOD1 by determination of the amino acid sequence of the peptides. The amino acid sequence of the peptide 92–122 was determined based on the assumption that Cys^{111} was modified with carbamidemethyl (Fig. 5*B*), sulfinic acid (SO_2H) (Fig. 5*C*), and sulfonic acid (SO_3H) (Fig. 5*D*), respectively. The mass of peptide *c* (3320.5 *m/z*), Cys-carbamidemethyl ($[M + 2H]^{2+}$ = 1661.2 *m/z*) gave the major fragment ions, y5 (611.3 *m/z*), y10 (1152.0 *m/z*), y12 (1424.6 *m/z*), y13 (1561.7 *m/z*), and y21* ($[M + 2H]^{2+}$ = 1161.0 *m/z*), indi-

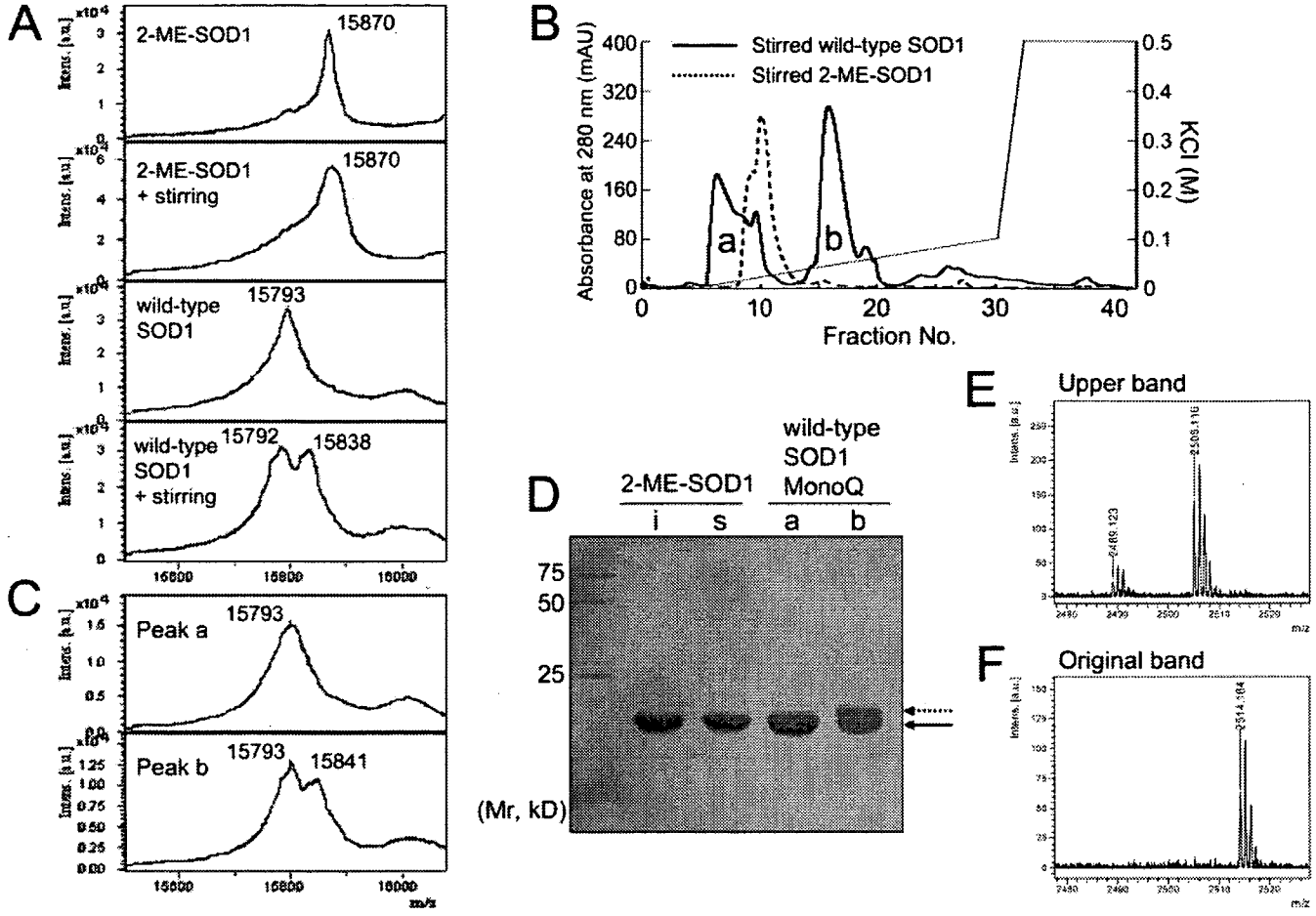

FIGURE 3. **Analyses of upper and original bands on SDS-PAGE.** *A*, MALDI-TOF MS spectra of intact and stirred 2-ME-SOD1 and wild-type SOD1, respectively. *B*, chromatogram profiles of stirred wild-type SOD1 and 2-ME-SOD1 on a MonoQ column. *C*, MALDI-TOF MS spectra of SOD1 in peaks *a* and *b*, separated with a MonoQ column (*B*). *D*, SDS-PAGE of intact (*i*) and stirred (*s*) 2-ME-SOD1 and SOD1s in peaks *a* and *b*. The *arrowheads* with *solid lines* indicate SOD1 subunits, and *arrowheads* with *broken lines* indicate modified SOD1 subunits. Precision Plus protein standards purchased from Bio Rad were used for the molecular weight marker (*left side*). *E* and *F*, MALDI-TOF MS spectra of tryptic peptides (residues Asp^{92}–Arg^{115}) from the upper band (*E*) and the original band (*F*), respectively, in the *right lane* of *D*. *mAU*, milliabsorbance units.

cating that Cys^{111} was carbamidemethylated, as expected (Fig. 5*E*). The mass of peptide *d* (3295.5 *m/z*) ([M + 2H]$^{2+}$ = 1648.3 *m/z*) gave the major fragment ions, y11 (1264.6, *m/z*), y12 (1399.7 *m/z*), y13 (1536.7 *m/z*), and b20 (2031.6 *m/z*), which was identified to be residues 92–122 containing Cys^{111}-SO_2H (Fig. 5*F*). Furthermore, the mass of peptide *e* (3311.6 *m/z*) ([M + 2H]$^{2+}$ = 1657.2 *m/z*) gave the major fragment ions, y9 (1038.6 *m/z*), y12 (1415.6 m/z), y13 (1552.7 *m/z*), y18 (2012.0 m/z), and y21 (2310.8 *m/z*), indicating that Cys^{111} was oxidized to Cys-SO_3H (Fig. 5*G*). Analyses based on the assumption that His^{110} and/or His^{120} were oxidized to 2-oxo-histidine showed that the corresponding y ions and b ions were absent (data not shown). These results clearly indicated that Cys^{111} was readily oxidized to Cys-SO_2H, which underwent further oxidation to Cys-SO_3H without His oxidation by air, and that the peroxidation of SOD1 at Cys^{111} resulted in the upper band shift in reducing SDS-PAGE.

Anti-C111ox-SOD1 Recognized Only Cys^{111}-peroxidized SOD1—To explore the possibility of immunological detection of Cys^{111}-peroxidized SOD1 (Cys^{111}-SO_3H-SOD1), a rabbit polyclonal antibody against the peptide containing Cys^{111}-SO_3H was prepared. The antiserum was purified to exclude the reactivity with reduced form SOD1 (Cys^{111}-SH) by affinity columns as described under "Experimental Procedures." The resultant IgG, which was denoted as anti-C111ox-SOD1, reacted with only the upper band of Cys^{111}-peroxidized SOD1 but neither the original band of wild-type SOD1 nor 2-ME-SOD1 (Fig. 6*A*). These data further demonstrated that the upper band is the oxidized form of SOD1 containing sulfonylated Cys^{111}. Also, in ELISA experiments, the anti-C111ox-SOD1 specifically reacted with IA-treated air-oxidized wild-type SOD1, but neither with 2-ME-SOD1 nor with IA-treated wild-type SOD1 (Fig. 6*B*). However, when wild-type SOD1 was not treated with IA before ELISA, the wild-type SOD1 was also reacted with anti-C111ox-SOD1, indicating that SH of Cys^{111} of the wild-type SOD1 was oxidized during coating on the 96-well plate.

Two-dimensional Gel Electrophoresis Characterization of Oxidized SOD1—It is well known that human, bovine, and recombinant human SOD1 proteins have several charge isomers detected by HPLC, isoelectric gel focusing, or two-dimensional gel electrophoresis (26, 30, 31). The reason for the heterogeneity is still unknown, although some hypotheses, such as different metallation, different conformation, and different oxidation of Cys residues, were presented (13, 26). Thus, two-dimensional gel electrophoresis of oxidized SOD1 was performed

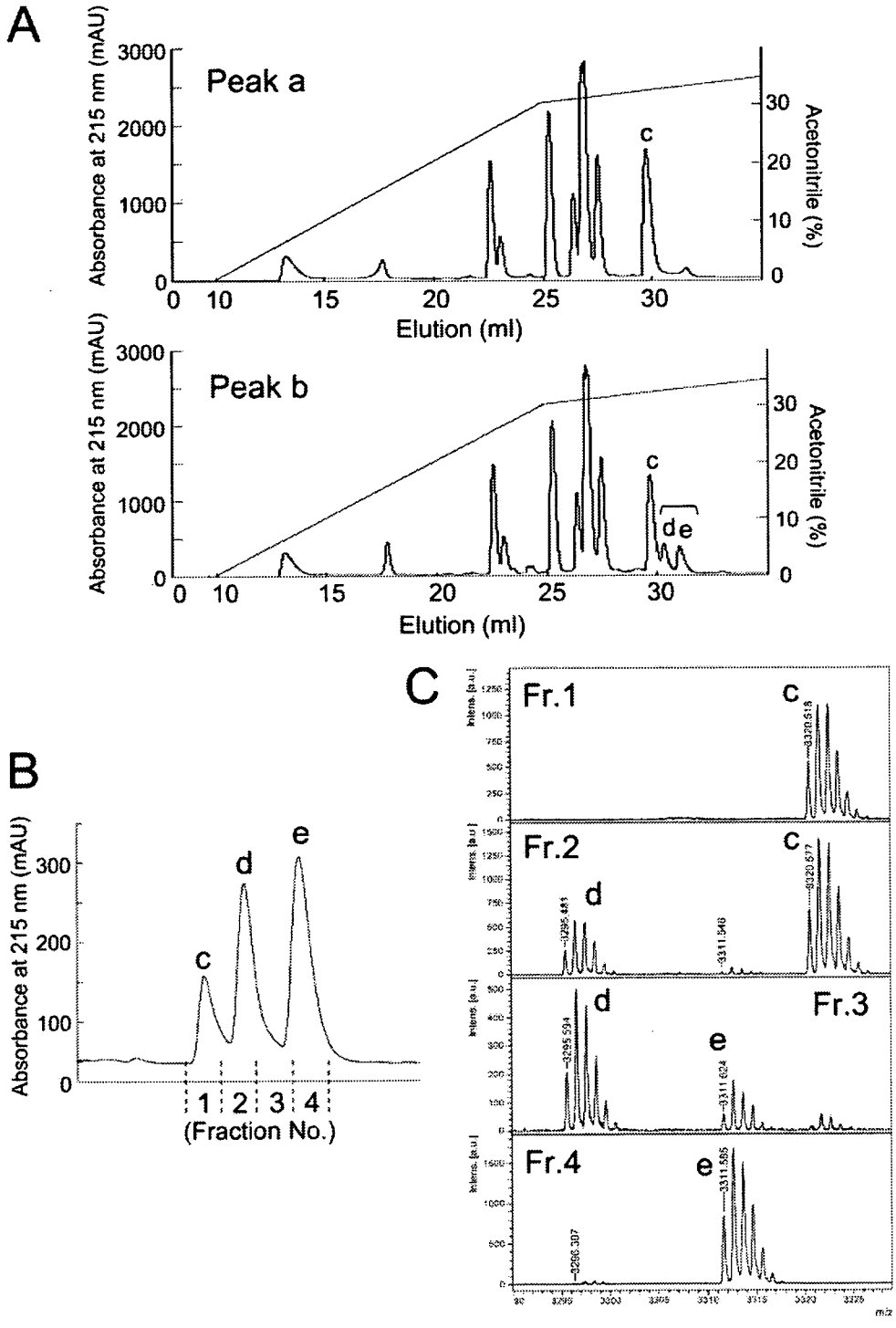

FIGURE 4. **Purification and analyses of lysylendopeptidase-digested peptides.** SOD1s in peaks *a* and *b* in Fig. 3*B* were digested with lysylendopeptidase after treatments with DTT and iodoacetamide, and the digests were fractionated by HPLC using a TSK-GEL ODS-80TM column. *A*, chromatogram profiles of the digests from peaks *a* (*top*) and *b* (*bottom*), separated with a MonoQ column (Fig. 3*B*). *B*, rechromatogram profile of fractions containing peaks *d* and *e*, at the *bottom* of *A*. *C*, MALDI-TOF MS spectra of peptides in factions 1–4 in *B*. *mAU*, milliabsorbance units.

to examine the effects of Cys^{111} oxidation on the generation of charge isomers. As shown in Fig. 7*A*, wild-type SOD1 presented the main spot *3* (pI 5.15) and three tiny spots, *1* (pI 4.92), *2* (pI 5.02), and *4* (pI 5.8). 2-ME-SOD1 also presented four similar spots (Fig. 7*B*). Three of them, spots *1–3*, were thought to correspond to three isomers of recombinant human SOD1 with pI of 4.99, 5.06, and 5.14, which was previously determined by isoelectric gel electrophoresis (30). When 2-ME-SOD1 was oxidized by H_2O_2, three major spots, *5* (pI 5.32), *6* (pI 5.52) and *7* (pI 5.65), were newly generated between spots *3* and *4* (Fig. 7*C*). In contrast, when wild-type SOD1 was oxidized by H_2O_2, further new spots, *5′* (pI 5.3), *6′* (pI 5.46), and *7′* (pI 5.6), which were probably their upper and acidic shifted spots of the spots *5* (pI 5.32), *6* (pI 5.52), and *7* (pI 5.65), respectively, were generated (Fig. 7, *D* and *E*). Furthermore, two major spots, *1′* and *2′*, and weak spot 3′, just above spots *1*, *2*, and *3*, respectively, were also detected by anti-C111ox-SOD1 (Fig. 7*E*). Air oxidation of wild-type SOD1 generated only the two major spots, *1′* and *2′*, and one tiny spot, *7′* (Fig. 7, *F* and *G*). Therefore, these results indicated that spots *1′*, *2′*, and 7′ were generated by the oxidation of Cys^{111} and that the generation of spots *5*, *6*, and *7* (Fig. 7*C*) was caused by the oxidation of other amino acid residues.

Cys^{111}-peroxidized SOD1 Was Detected in Spinal Cord of G1H-G93A Mice—Because this new antibody, anti-C111ox-SOD1, is a good tool for detection of Cys^{111}-peroxidized SOD1, G1H-G93A mouse spinal cord extract was subjected to Western blot analysis to examine the involvement of oxidized SOD1 in ALS. The anti-C111ox-SOD1 clearly reacted with the ~25 kDa band in the Triton X-100-soluble fraction (Fig. 8*A*, *left*). Although some weak bands were detected, the upper band of oxidized SOD1 was not detected in all fractions. Immunostaining with anti-SOD1 detected a large amount of human SOD1 overexpressed in the G1H-G93A mouse and mouse SOD1 (Fig. 8*A*, *right*). In contrast, anti-C111ox-SOD1 detected the upper band of oxidized SOD1 (positive control) but neither the reduced form of G93A-SOD1 nor mouse SOD1 (Fig. 8*A*, *left*). Therefore, the 25 kDa band, selectively recognized by anti-C111ox-SOD1, was thought to be some molecule-bound oxidized SOD1. Basso *et al.* (26) detected mono- and polyubiquitinated SOD1 (24, 32, 40, 48 kDa spots in two-dimensional gel electrophoresis) in the Triton X-100-insoluble

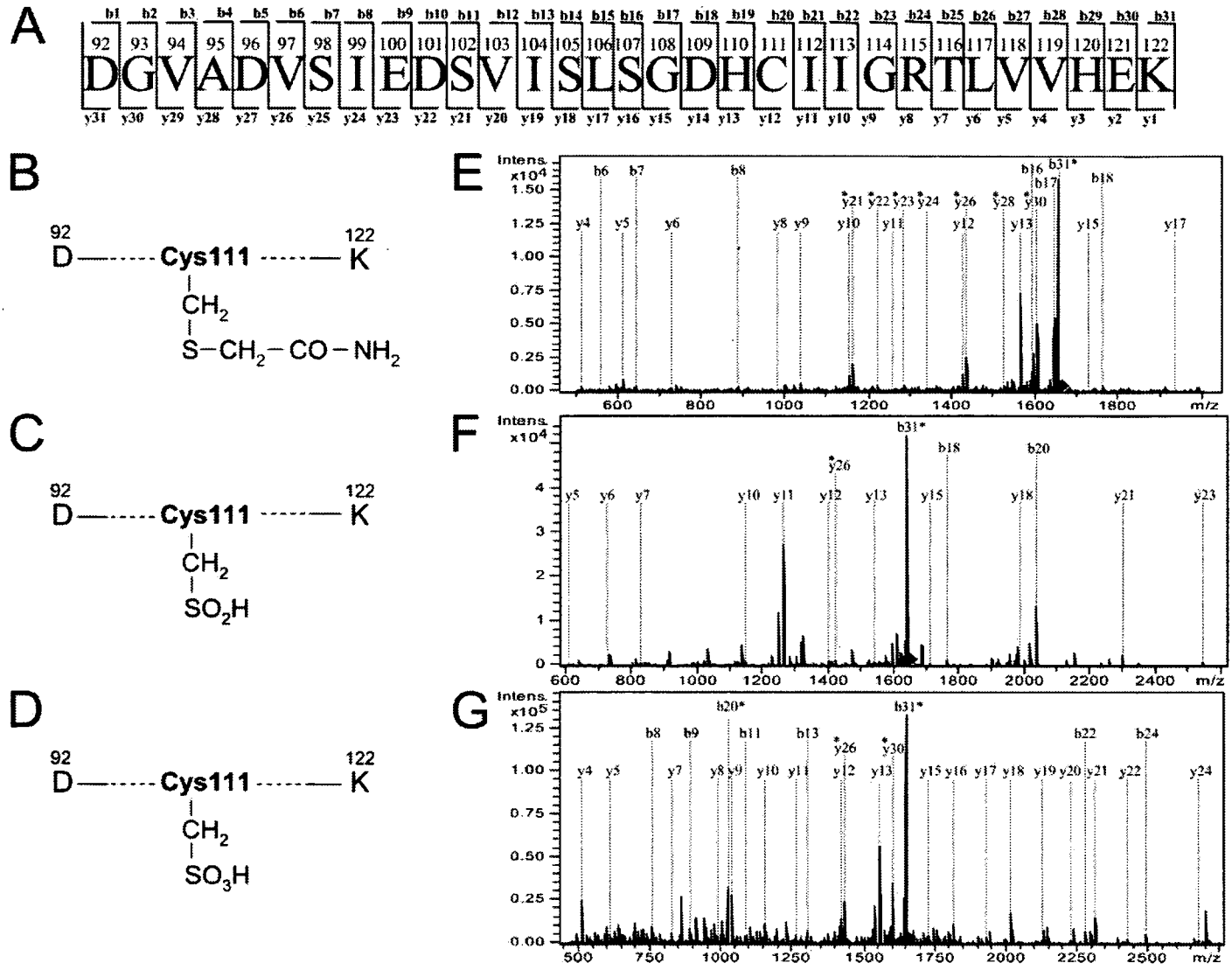

FIGURE 5. **Sequence analysis of modified peptide 92–122 by ESI MS.** *A*, schematic representation of peptides obtained from fragmentations by MS/MS analysis. *B–D*, Cys modification observed in this experiment. Carbamidemethyl-Cys (*B*), sulfinyl Cys (C-SO_2H) (*C*), and sulfonyl Cys (C-SO_3H) (*D*). *E–G*, MS/MS sequence analysis of the peptide 92–122 digested with lysylendopeptidase in fractions 1, 3, and 4 (*B*). *E*, MS/MS analysis of the peptide modified with carbamidemethyl-Cys ($[M + 2H]^{2+}$ = 1661.2 *m/z*) in fraction 1. *F*, MS/MS analysis of the peptide modified with C-SO_2H ($[M + 2H]^{2+}$ = 1648.3 m/z) in fraction 3. *G*, MS/MS analysis of the peptide modified with C-SO_3H ($[M + 2H]^{2+}$ = 1657.2 m/z) in fraction 4. The y-ions and b-ions labeled with *asterisks* are the doubly charged ions. The mass number labeled with *diamond* is that of the precursor ion in *E–G*.

fraction of G93A transgenic mice spinal cords. Thus, the 25 kDa band was speculated to be monoubiquitinated SOD1, and then the immunostaining with anti-ubiquitin on the same membrane was performed. Although the 25 kDa band appeared to be one of the ubiquitinated proteins (data not shown), evidence of monoubiquitination has not been obtained. We are currently exploring the identity of the molecule bound to Cys^{111}-peroxidized SOD1. Finally, an immunohistochemical study of paraffin-embedded spinal cord sections of G1H-G93A mice was performed. The G1H-G93A mice examined at 110 days of age revealed severe loss of anterior horn cells with gliosis and both Lewy body-like hyaline inclusions (LBHIs) and vacuolation pathologies (32). The anti-C111ox-SOD1 selectively labeled the LBHIs in the neuropil and in the cytoplasm of the neurons (Fig. 8*B*) and the rim of the vacuoles in the neuropil (Fig. 8*C*). When the paraffin sections were incubated with BSA-PBS alone or with anti-C111ox-SOD1 pretreated with an excess amount of air-oxidized SOD1 or peptide containing sulfonylated Cys^{111}, no staining was detected. The spinal cords of the two littermates exhibit neither distinct histopathological changes nor staining with anti-C111ox-SOD1. These results suggested that the Cys^{111}-peroxidized SOD1 was involved in the formation of the LBHIs and the vacuoles in ALS spinal cords.

DISCUSSION

Because SOD1 catalyzes the conversion of superoxide radicals into molecular oxygen and hydrogen peroxide, SOD1 is thought to be a major target of oxidative stress. The results of this study show that the Cys^{111} residue plays an important role in oxidative fragmentation and aggregation of human SOD1 (Fig. 2). Moreover, the upper shifted band on reducing SDS-PAGE generated after oxidation (Fig. 1) was determined to be an oxidized SOD1 subunit containing sulfinic acid (Cys^{111}-

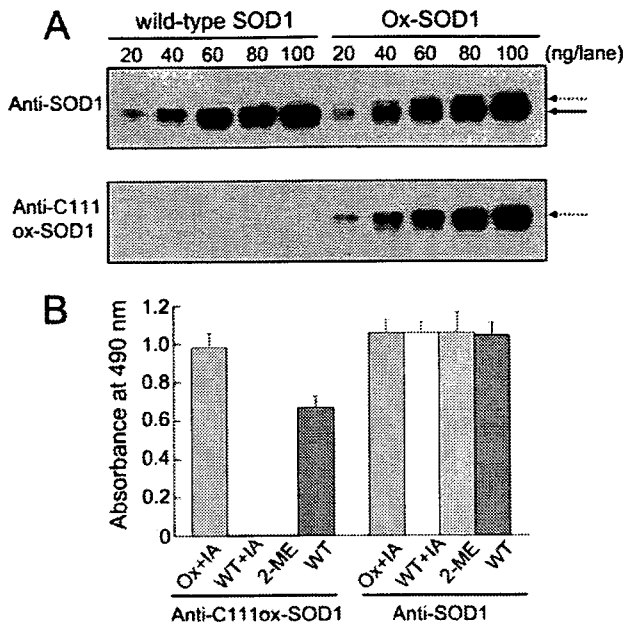

FIGURE 6. **Validation of anti-C111ox-SOD1 that selectively recognizes Cys^{111}-peroxidized SOD1.** *A*, Western blot analyses for 2-ME-SOD1 and air-oxidized SOD1 detected by anti-SOD1 (*top*) and anti-C111ox-SOD1 (*bottom*). An *arrowhead* with *solid lines* indicates wild-type SOD1 subunits, and *arrowheads* with *broken lines* indicate Cys^{111}-peroxidized SOD1 subunits. The PVDF membrane was first reacted with anti-C111ox-SOD1. The antibody was stripped from the membrane, which was reincubated with anti-SOD1. *B*, ELISA for 2-ME-SOD1 and air-oxidized SOD1 treated with and without IA detected by anti-C111ox-SOD1 (*left*) and anti-SOD1 (*right*). *Ox*, *WT*, and *2-ME*, air-oxidized SOD1, wild-type SOD1, and 2-ME-SOD1, respectively. Data are presented as the means ± S.D. of triplicate experiments.

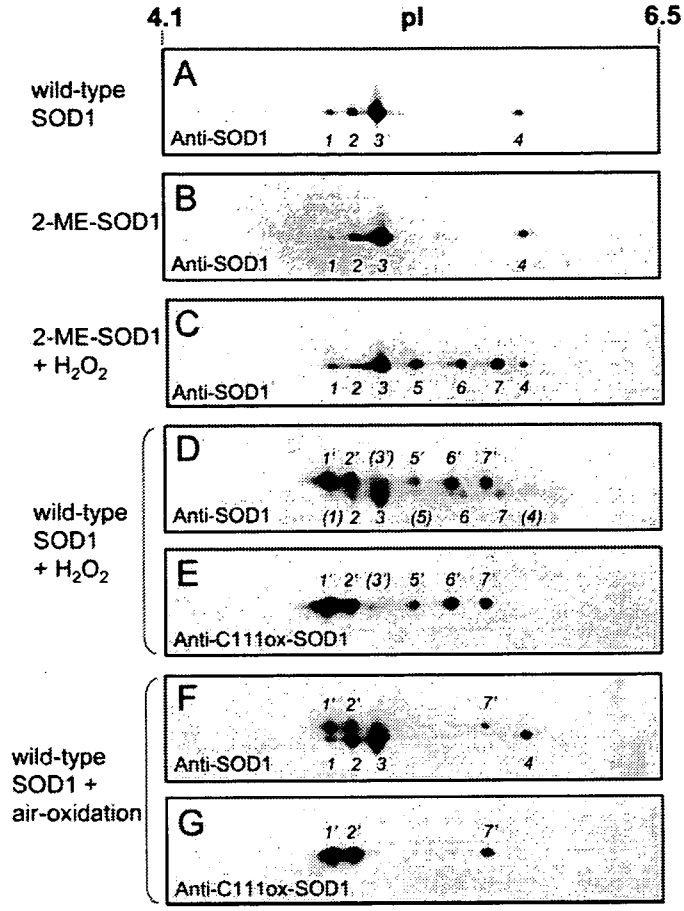

FIGURE 7. **Two-dimensional Western blot analyses for wild-type and 2-ME SOD1s with and without oxidation detected by anti-SOD1 (*A–D* and *F*) and anti-C111ox-SOD1 (*E* and *G*).** 5 μg of SOD1s treated with and without 1 mM H_2O_2 for 1 h or with air oxidation for 24 h were subjected to two-dimensional gel electrophoresis and Western blot analysis. The PVDF membrane was first reacted with anti-C111ox-SOD1. The antibody was stripped from the membrane, which was reincubated with anti-SOD1.

SO_2H) and sulfonic acid (Cys^{111}-SO_3H) (Figs. 3–5). The newly developed specific antibody against a peptide containing Cys^{111}-SO_3H, anti-C111ox-SOD1, recognized the upper band (Cys^{111}-SO_3H form) but not the original band (Cys^{111}-SH form) by Western blot analyses (Figs. 6–8). These results further demonstrated that the upper band is the oxidized form of SOD1 containing Cys^{111}-SO_3H. Although the increment in the mass, 32 or 48, is small, oxidized SOD1 has slower mobility on the SDS-PAGE. This phenomenon is, however, frequently observed in SOD1. For example, mutant G85R has faster mobility in SDS-PAGE, although the difference in the mass is 99 (33). Mouse SOD1 also has faster mobility than human SOD1 in SDS-PAGE, although both SOD1s have similar molecular weight (Fig. 8*A*).

Some cysteine residues are sensitive to oxidation, because their environment promotes ionization of the thiol (Cys-SH) group, even at a neural pH, to the thiolate anion (Cys-S$^-$), which is more readily oxidized to sulfenic acid (Cys-SOH) than is Cys-SH (34, 35). The sulfenic acid group generally is unstable and reacts with any accessible thiol to form a disulfide (S-S) bond, or sulfenic acid may undergo further oxidation to sulfinic acid (Cys-SO_2H) and to sulfonic acid (Cys-SO_3H) in the presence of strong oxidants (34). In the active site of some proteins, such as Prx and thioredoxin, one cysteine is in the thiolate form and, as a result, can react with H_2O_2 (36, 37). In the case of PrxI, Cys^{51} is selectively oxidized to Cys-SO_2H but not to Cys-SO_3H, as evidenced by the difference of 32 mass units between reduced and oxidized PrxI proteins. Additional oxidation with H_2O_2 did not increase Cys-SO_3H even *in vitro* (22, 34). Cys^{51}-SO_2H is rereduced to Cys^{51}-SH by sulfiredoxin but not by DTT or thioredoxin (23, 38). In contrast, in intact human SOD1, Cys^{111} appears to be oxidized to Cys^{111}-SO_3H, even by mild oxidation in air. As shown in this study, air oxidation of SOD1 resulted in two proteins with a mass unit difference of about 48 (*i.e.* three oxygen atoms) (Fig. 3). Oxidation of Cys^{111} occurred above pH 7, suggesting that Cys^{111} is in the thiolate form at physiological pH and can therefore react not only with H_2O_2 but also with oxygen in ambient air (Fig. 1). Cys^{111} also is readily modified with *N*-ethylmaleimide or 4-vinylpyridine (29, 39) or bound to another sulfhydryl, such as 2-ME (supplemental Fig. S1) or cysteine (39). In contrast, the free cysteine at residue 6, Cys^6, is less reactive with oxygen, 2-ME, or *N*-ethylmaleimide (present study) (29), probably because it exists in β-sheet 1a and is buried within the SOD1 molecule (40). In other studies, exposure of bovine SOD1 to an excess of H_2O_2 resulted in selective oxidation of His^{118} (corresponding to His^{120} in human SOD1), inactivating the enzyme (2). Rakhit *et al.* (6) showed that four amino acids (His^{48}, His^{80}, His^{120}, and Phe^{20}) in human SOD1 were prone to oxidation by ascorbic acid/$CuCl_2$. However, neither oxidation of His^{120} in wild-type SOD1 (Fig. 5) nor change in mass of 2-ME-SOD1 (Fig. 3) by air oxidation was observed. These results indicate that most amino acids in human SOD1

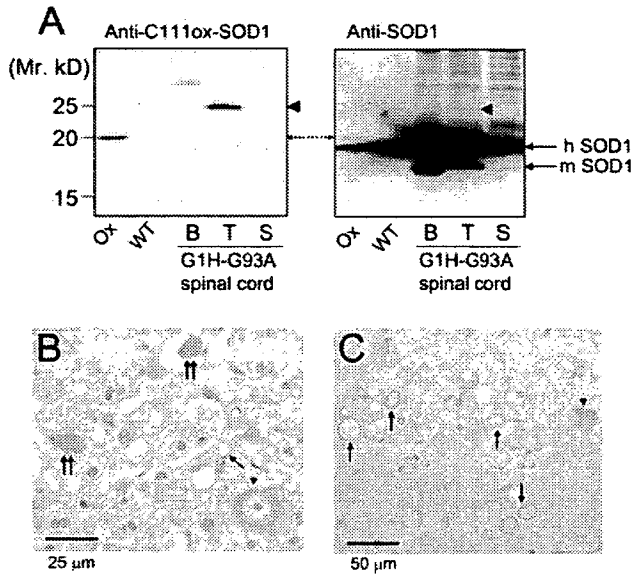

FIGURE 8. **Cys^{111}-peroxidized SOD1 in spinal cord of G1H-G93A mice.** *A*, Western blot analyses for G1H-G93A spinal cord extracts detected by anti-C111ox-SOD1 (*left*) and anti-SOD1 (*right*). 60 μg of proteins of buffer-soluble (*B*), Triton X-100-soluble (*T*), and SDS-soluble (*S*) fractions, respectively, were applied. The *arrowheads* with *solid lines* indicate human and mouse SOD1 subunits, and a *double arrowhead* with a *broken line* indicates Cys^{111}-peroxidized SOD1 subunits. The *arrowheads* indicate a 25 kDa band reacted with anti-C111ox-SOD1. 20 ng of air-oxidized SOD1 (*Ox*) and wild-type SOD1 (*WT*) were applied as controls. The PVDF membrane was first reacted with anti-C111ox-SOD1. The antibody was stripped from the membrane, which was reincubated with anti-SOD1. Precision Plus protein standards purchased from Bio-Rad were used as molecular weight markers. *B* and *C*, immunohistochemical analyses of paraffin-embedded G1H-G93A spinal cord sections detected by anti-C111ox-SOD1. *B*, *double arrows* indicate LBHIs in the neuropil and in the cytoplasm of the neurons immunostained with anti-C111ox-SOD1. A *single arrow* indicates a rim of the vacuoles in the neuropil immunostained with anti-C111ox-SOD1. An *arrowhead* indicates the surviving motor neuron, which is not stained with anti-C111ox-SOD1. *Scale bar*, 25 μm. *C*, *single arrows* indicate rims of vacuoles detected by anti-C111ox-SOD1. An *arrowhead* indicates the surviving motor neuron, which is not stained with anti-C111ox-SOD1. *Scale bar*, 50 μm.

are not oxidized by air, the exception being Cys^{111}. Therefore, these findings demonstrate that, in human SOD1, Cys^{111} is the most reactive and sensitive amino acid to oxygen and other oxidizing agents.

The oxidation of Cys^{51}-SH to Cys^{51}-SO_2H causes acidic shifting of PrxI upon two-dimensional gel electrophoresis (22). In contrast, human, bovine, and recombinant human SOD1 originally have some charge isomers before oxidation (30, 31). Fig. 7, *A* and *B*, also showed that both wild-type SOD1 and 2-ME-SOD1 have four similar spots, although they have their own mass. Cys^{111} oxidation by air oxidation generated two major spots, *1'* and *2'*, just above the two minor isomers, *1* and *2* (pI 4.92 and 5.02) (Fig. 7, *F* and *G*). However, these spots appear like acidic shifted spots of original main spot *3* (pI 5.15), because no spot above the main spot was generated by air oxidation. These results suggest that peroxidation of Cys^{111} also causes acidic shifting of SOD1. Further oxidation by H_2O_2 further generated several spots, and a total of 13 spots were observed on two-dimensional gel electrophoresis (Fig. 7*D*). Therefore, isomers of SOD1 observed in the previous reports (13, 26) may be due to both oxidative modification and charge isomers of SOD1 itself.

Although more than 110 FALS mutations in the SOD1 have been identified, the mechanism by which the FALS-linked mutant SOD1s cause motor neuron degeneration is not completely understood. Two hypotheses have been proposed explaining the toxic gain of function that is associated with these mutations (12, 41). The "copper hypothesis" proposes that copper, either bound to or released from FALS-linked mutant SOD1s generates reactive oxygen species harmful to motor neurons (42–44). The "aggregation hypothesis" supposes that FALS-linked mutant SOD1s are structurally unstable and tend to aggregate, resulting in degeneration of neuronal cells analogous to that observed in other neurodegenerative disorders such as Alzheimer, Parkinson, and Huntington diseases (33, 45, 46). However, recent reports suggest that these two hypotheses are interrelated. Copper ion oxidized Cys^{111} in human SOD1 (Fig. 1). Oxidation may result in misfolding and aggregation even in wild-type SOD1 (6, 47). Oxidized wild-type SOD1 exhibits characteristics of FALS-linked mutant SOD1s: conjugation with polyubiquitin, interaction with Hsp70 or chromogranin B, and toxic effects on motor neurons (7). Although this study demonstrated that the SH of Cys^{111} underwent irreversible peroxidation to Cys-SO_2H and to Cys-SO_3H, Cys^{111} may also participate in disulfide bond linkage with other cysteine residues and oligomerization (48). Furukawa *et al.* (49–51) showed that incorrect intermolecule disulfide cross-linking of immature, misfolded FALS-linked mutant SOD1s leads to formation of insoluble aggregates. On the other hand, an immunohistochemical study using the anti-C111ox-SOD1 revealed that Cys^{111}-peroxidized mutant SOD1 accumulated in the vacuole structures and LBHIs (Fig. 8, *B* and *C*). Because the most characteristic neuropathological findings in ALS model mice are LBHIs and vacuoles (32, 33), the peroxidation of Cys^{111} may contribute to the pathology of the degeneration/death of FALS motor neurons. However, the amount of the Cys^{111}-peroxidized SOD1 appears to be quite limited (Fig. 8*A*). Large quantities of thiol compounds, such as glutathione and cysteine, probably protect the SH of Cys^{111} in healthy cells. The surviving neuron cells were not immunostained by anti-C111ox-SOD (Fig. 8, *B* and *C*). Ferri *et al.* (48) proposed that Cys^{111} was a key mediator of mitochondrial association of SOD1 and subsequent mitochondrial dysfunction, because the C111S mutant was less associated with mitochondria. Recently, it was also reported that A4V/C111S protein was more stable than A4V protein in cells (52). However, it is still an open question whether Cys^{111} is essential for the etiology of ALS, because mice that express mouse SOD1-G85R developed ALS-like symptoms, although Ser, not Cys, is at residue 111 of mouse SOD1 (53). It is thought that Cys^{111} may enhance human ALS development. A comparative study of symptoms between mice expressing the ALS mutation with C111S (G93A/C111S etc.) and traditional ALS model mice (G93A etc.) would answer the question.

In summary, we demonstrated that Cys^{111} in human SOD1 is a primary target for oxidation and is readily oxidized to Cys^{111}-SO_3H. The specific antibody against the Cys^{111}-SO_3H will be a useful tool for detecting oxidized human SOD1. Precise studies of the role of oxidized SOD1 in ALS are currently under way.

Acknowledgments—We are grateful to Ube Industries Ltd. for kindly providing the 2-ME-SOD1. We thank Dr. Kentaro Ihara (High Energy Accelerator Research Organization) for helpful discussion.

REFERENCES

1. Hodgson, E. K., and Fridovich, I. (1975) *Biochemistry* **14,** 5299–5303
2. Uchida, K., and Kawakishi, S. (1994) *J. Biol. Chem.* **269,** 2405–2410
3. Kurahashi, T., Miyazaki, A., Suwan, S., and Isobe, M. (2001) *J. Am. Chem. Soc.* **123,** 9268–9278
4. Salo, D. C., Pacifici., R. E., Lin, S. W., Giulivi, C., and Davies, K. J. (1990) *J. Biol. Chem.* **265,** 11919–11927
5. Ookawara, T., Kawamura, N., Kitagawa, Y., and Taniguchi, N. (1992) *J. Biol. Chem.* **267,** 18505–18510
6. Rakhit, R., Cunningham, P., Furtos-Matei, A., Dahan, S., Qi, X.-F., Crow, J. P., Cashman, N. R., Kondejewski, L. H., and Chakrabartty, A. (2002) *J. Biol. Chem.* **277,** 47551–47556
7. Ezzi, S. A., Urushitani, M., and Julian, J. P. (2007) *J. Neurochem.* **102,** 170–178
8. Zhang, H., Andrekopoulos, C., Joseph, J., Chandran, K., Karoui, H., Crow, J. P., and Kalyanaraman, B. (2003) *J. Biol. Chem.* **278,** 24078–24089
9. Deng, H. X., Hentati, A., Tainer, J. A., Zafar, I., Cayabyab, A., Hung, W. Y., Getzoff, E. D., Hu, P., Herzfeldt, B., Roos, R. P., Warner, C., Deng, G., Soriano, E., Smyth, C., Parge, H. E., Ahmed, A., Roses, A. D., Hallewell, R. A., Pericak-Vance, M. A., and Siddique, T. (1993) *Science* **261,** 1047–1051
10. Rosen, D. R., Siddique, T., Patterson, D., Figlewicz, D. A., Sapp, P., Hentati, A., Donaldson, D., Goto, J., O'Regan, J. P., Deng, H. X., Rahmani, Z., Krizus, A., McKenna-Yasek, D., Cayabyab, A., Gaston, S. M., Berger, R., Tanzi, R. E., Halperin, J. J., Herzfeldt, B., Van den Bergh, R., Hung, W. Y., Bird, T., Deng, G., Mulder, D. W., Smyth, C., Laing, N. G., Soriano, E., Pericak-Vance, M. A., Hains, J., Rouleau, G. A., Gusella, J. S., Horvitz, H. R., and Brown, R. H., Jr. (1993) *Nature* **362,** 59–62
11. Julien, J. P. (2001) *Cell* **104,** 581–591
12. Valentine, J. S., and Hart, P. J. (2003) *Proc. Natl. Acad. Sci. U. S. A.* **100,** 3617–3622
13. Choi, J., Rees, H. D., Weintraub, S. T., Levey, A. I., Chin, L.-S., and Li, L. (2005) *J. Biol. Chem.* **280,** 11648–11655
14. Tainer, J. A., Getzoff, E. D., Beem, K. M., Richardson, J. S., and Richardson, D. C. (1982) *J. Mol. Biol.* **160,** 181–217
15. Parge, H. E., Hallewell, R. A., and Tainer, J. A. (1992) *Proc. Natl. Acad. Sci. U. S. A.* **89,** 6109–6113
16. Fink, R. C., and Scandaliios, J. G. (2002) *Arch. Biochem. Biophys.* **399,** 19–36
17. Fukuhara, R., Tezuka, T., and Kageyama, T. (2002) *Gene (Amst.)* **296,** 99–109
18. Stanton, J. L., Wilton, S. D., and Laing, N. G. (1996) *DNA Seq.* **6,** 357–360
19. Repock. J. R., Frey, H. E., and Hallewell, R. A. (1990) *J. Biol. Chem.* **265,** 21612–21618
20. De Beus, M. D., Chung, J., and Colon, W. (2004) *Protein Sci.* **13,** 1347–1355
21. Jacob, C., Holme, A. L., and Fry, F. H. (2004) *Org. Biomol. Chem.* **2,** 1953–1956
22. Yang, K.-S., Kang, S. W., Woo, H. A., Hwang, S. C., Chae, H. Z., Kim, K., and Rhee, S. G. (2002) *J. Biol. Chem.* **277,** 38029–38036
23. Woo, H. A., Jeong, W., Chang, T.-S., Park, K. J., Park, S. J., Yang, J. S., and Rhee, S. G. (2005) *J. Biol. Chem.* **280,** 3125–3128
24. Hallewell, R. A., Imlay, K. C., Lee, P., Fong, N. M., Gallegos, C., Getzoff, E. D., Tainer, J. A., Cabelli, D. E., Tekamp-Olson, P., Mullenbach, G. T., and Cousens L. S. (1991) *Biochem. Biophys. Res. Commun.* **181,** 474–480
25. Fujiwara, N., Miyamoto, Y., Ogasahara, K., Takahashi, M., Ikegami, T., Takamiya, R., Suzuki, K., and Taniguchi, N. (2005) *J. Biol. Chem.* **280,** 5061–5070
26. Basso, M., Massignan, T., Samengo, G., Cheroni, C., De Biasi, S., Salmona, M., Bendotti, C., and Bonetto, V. (2006) *J. Biol. Chem.* **281,** 33325–33335
27. McCord, J. M., and Fridovich, I. (1969) *J. Biol. Chem.* **244,** 6049–6055
28. Goto, J. J., Gralla, E. B., Valentine, J. S., and Cabelli, D. E. (1998) *J. Biol. Chem.* **273,** 30104–30109
29. Okado-Matsumoto, A., Guan, Z., and Fridovich, I. (2006) *Free Radic. Biol. Med.* **41,** 1837–1846
30. Kajihara, J., Enomoto, M., Seya, K., Sukenaga, Y., and Katoh, K. (1998) *J. Biochem. (Tokyo)* **104,** 638–642
31. Kajihara, J., Enomoto, M., Nishijima, K., Yabuuchi, M., and Katoh, K. (1998) *J. Biochem. (Tokyo)* **104,** 851–854
32. Kato, S., Kato, M., Abe, Y., Matsumura, T., Nishino, T., Aoki, M., Itoyama, Y., Asayama, K., Awaya, A., Hirano, A., and Ohama, E. (2005) *Acta Neuropathol.* **110,** 101–112
33. Bruijn, L. I., Houseweart, M. K., Kato, S., Anderson, K. L., Anderson, S. D., Ohama, E., Reaume, A. G., Scott, R. W., and Cleveland D. W. (1998) *Science* **281,** 1851–1854
34. Woo, H. A., Chae, H. Z., Hwang, S. C., Yang, K.-S., Kang, S. W., Kim, K., and Rhee, S. G. (2003) *Science* **300,** 653–656
35. Kim, J. R., Yoon, H. W., Kwon, K. S., Lee, S. R., and Rhee, S. G. (2000) *Anal. Biochem.* **283,** 214–221
36. Rhee, S. G., Kang, S. W., Chang, T. S., Jeong, W., and Kim, K. (2001) *IUBMB Life* **52,** 35–41
37. Forman, H. J., Torres, M., and Fukuto, J. (2002) *Mol. Cell Biochem.* **234,** 49–62
38. Chang, T. S., Jeong, W., Woo. H. A., Lee, S. M., Park, S., and Rhee, S. G. (2004) *J. Biol. Chem.* **279,** 50994–51001
39. Liu, H., Zhu, H., Eggers, D. K., Nersissian, A. M., Faull, K. F., Goto, J. J., Ai, J., Sanders-Loehr, J., Gralla, E. B., and Valentine, J. S. (2000) *Biochemistry* **39,** 8125–8132
40. Getzoff, E. D., Tainer, J. A., Stempien, M. M., Bell, G. I., and Hallewell R. A. (1989) *Proteins* **5,** 322–336
41. Cleveland, D. W., and Rothstein, D. (2001) *Nat. Rev. Neurosci.* **2,** 806–819
42. Yim, M. B., Kang, J. H., Yim, H. S., Kwak, H. S., Chock, P. B., and Stadtman, E. R. (1996) *Proc. Natl. Acad. Sci. U. S. A.* **93,** 5709–5714
43. Ghadge, G. D., Lee, J. P., Bindokas, V. P., Jordan, J., Ma, L., Miller, R. J., and Roos, R. P. (1997) *J. Neurosci.* **17,** 8756–8766
44. Wiedau-Pazos, M., Goto, J. J., Rabizadeh, S., Gralla, E. B., Roe, J. A., Lee, M. K., Valentine, J. S., and Bredesen, D. E. (1996) *Science* **271,** 515–518
45. Johnston, J. A., Dalton, M. J., Gurney, M. E., and Kopito, R. R. (2000) *Proc. Natl. Acad. Sci. U. S. A.* **97,** 12571–12576
46. Stefani, M., and Dobson, C. M. (2003) *J. Mol. Med.* **81,** 678–699
47. Rakhit, R., and Chakrabartty, A. (2006) *Biochim. Biophys. Acta* **1726,** 1025–1037
48. Ferri, A., Cozzolino, M., Crosio, C., Nencini, M., Casciati, A., Gralla, E. D., Rotilio, G., Valentine, J. S., and Carrì, M. T. (2006) *Proc. Natl. Acad. Sci. U. S. A.* **103,** 13860–13865
49. Furukawa, Y., and O'Halloran, T. V. (2005) *J. Biol. Chem.* **280,** 17266–17274
50. Furukawa, Y., Fu, R., Deng, H. X., Siddique, T., and O'Halloran, T. V. (2006) *Proc. Natl. Acad. Sci. U. S. A.* **103,** 7148–7153
51. Deng, H. X., Shi, Y., Furukawa, Y., Zhai, H., Fu, R., Liu, E., Gorrie, G. H., Khan, M. S., Hung, W. Y., Bigio, E. H., Lukas, T., Dal Canto, M. C., O'Halloran, T. V., and Siddique, T. (2006) *Proc. Natl. Acad. Sci. U. S. A.* **103,** 7142–7147
52. Watanabe, S., Nagano, S., Duce, J., Kiaei, M., Li, Q. X., Tucker, S. M., Tiwari, A., Brown, R. H., Jr., Beal, M. F., Hayward, L. J., Culotta, V. C., Yoshihara, S., Sakoda, S., and Bush, A. I. (2007) *Free Radic. Biol. Med.* **42,** 1534–1542
53. Ripps, M. E., Huntley, G. W., Hof, P. R., Morrison, J. H., and Gordon, J. W. (1995) *Proc. Natl. Acad. Sci. U. S. A.* **92,** 689–693

JOURNAL OF VIROLOGY, Aug. 2007, p. 7902–7912 Vol. 81, No. 15
0022-538X/07/$08.00+0 doi:10.1128/JVI.02675-06

Establishment of a Poliovirus Oral Infection System in Human Poliovirus Receptor-Expressing Transgenic Mice That Are Deficient in Alpha/Beta Interferon Receptor▽

Seii Ohka,[1]* Hiroko Igarashi,[1] Noriyo Nagata,[2] Mai Sakai,[1] Satoshi Koike,[3] Tomonori Nochi,[4] Hiroshi Kiyono,[4] and Akio Nomoto[1]

Department of Microbiology, Graduate School of Medicine, The University of Tokyo, 7-3-1 Hongo, Bunkyo-ku, Tokyo 113-0033,[1] Department of Pathology, National Institute of Infectious Diseases, Gakuen 4-7-1, Musashimurayama-shi, Tokyo 208-0011,[2] Department of Microbiology, Tokyo Metropolitan Institute for Neuroscience, 2-6 Musashidai, Fuchu, Tokyo 183-8526,[3] and Division of Mucosal Immunology, Department of Microbiology and Immunology, The Institute of Medical Science, The University of Tokyo, 4-6-1 Shirokanedai, Minato-ku, Tokyo 108-8639,[4] Japan

Received 4 December 2006/Accepted 8 May 2007

Poliovirus (PV) is easily transferred to humans orally; however, no rodent model for oral infections has been developed because of the alimentary tract's low sensitivity to the virus. Here we showed that PV is inactivated by the low pH of the gastric contents in mice. The addition of 3% $NaHCO_3$ to the viral inoculum increased the titer of virus reaching the small intestine through the stomach after intragastric inoculation of PV. Transgenic mice (Tg) carrying the human PV receptor (hPVR/CD155) gene and lacking the alpha/beta interferon receptor (IFNAR) gene (hPVR-Tg/*Ifnar*KO) were sensitive to the oral administration of PV with 3% $NaHCO_3$, whereas hPVR-Tg expressing IFNAR were much less sensitive. The virus was detected in the epithelia of the small intestine and proliferated in the alimentary tract of hPVR-Tg/*Ifnar*KO. By the ninth day after the administration of a virulent PV, the mice had died. These results suggest that IFNAR plays an important role in determining permissivity in the alimentary tract as well as the generation of virus-specific immune responses to PV via the oral route. Thus, hPVR-Tg/*Ifnar*KO are considered to be the first oral infection model for PV, although levels of anti-PV antibodies were not elevated dramatically in serum and intestinal secretions of surviving mice when hPVR-Tg/*Ifnar*KO were administered an attenuated PV.

Poliomyelitis is an acute disease of the central nervous system (CNS) caused by poliovirus (PV), a human enterovirus that belongs to the family *Picornaviridae*. In humans, an infection is initiated by oral ingestion of the virus, followed by multiplication in the alimentary mucosa (2, 38), from which the virus spreads through the bloodstream. Viremia is considered essential for leading to paralytic poliomyelitis in humans. By use of a PV-sensitive mouse model, previous studies (9, 44) demonstrated that after intravenous inoculation, circulating PV crosses the blood-brain barrier at a high rate, and a neural dissemination pathway from the skeletal muscle without injury is not the primary route by which the circulating virus disseminates to the CNS. Along with the blood-brain barrier pathway of dissemination, a neural pathway has been reported for humans (30), primates (11), and PV-sensitive transgenic mice (Tg) carrying the human PV receptor (hPVR/CD155) gene (31, 34); this pathway appears to be important in causing provocation poliomyelitis (9).

It has been proved that Tg carrying the hPVR gene (hPVR-Tg) are susceptible to all three PV serotypes, 1, 2, and 3 (22, 35), although mice without the hPVR gene are generally not susceptible to PV. This observation indicates that hPVR is the most important determinant of the host range of PV. After inoculation with PV by the intracerebral, intraspinal, intravenous, or intramuscular route (10, 20–22, 33–35), hPVR-Tg develop a flaccid paralysis in their limbs, which is clinically similar to human poliomyelitis. However, in contrast to its behavior in humans, PV does not replicate in the alimentary tracts of hPVR-Tg after oral administration, even in animals expressing high levels of hPVR in the intestinal epithelial cells (45). This result suggests that the expression of hPVR in the intestine is not solely responsible for the infection. It is also known that nonhuman primates are highly susceptible to PV by all routes except the oral route, yet the degree of oral susceptibility depends on the species (12). Thus, although oral infection is the most important route in humans, no adequate animal model has been established so far.

After an oral infection with PV, the virus must overcome at least three barriers before it can start to replicate efficiently in the first target cells in the small intestine: (i) the gastric acid solution, by which PV may be inactivated; (ii) inappropriate distribution of hPVR, by which PV may not be ushered to the correct target cells; and (iii) innate immunity, including interferon (IFN) signaling, by which the replication of PV may be hampered in the target cells (7). To know why orally administered PV hardly causes any paralysis in animals other than humans, we have to verify each step (see Fig. 7). In this report, barrier ii is defined as cell susceptibility and barrier iii is defined as cell permissivity.

To control poliomyelitis, attenuated PV strains of all three serotypes have been developed and used effectively as oral polio vaccines (37, 39). The attenuated Sabin strains can rep-

* Corresponding author. Mailing address: Department of Microbiology, Graduate School of Medicine, The University of Tokyo, 7-3-1 Hongo, Bunkyo-ku, Tokyo, 113-0033, Japan. Phone: 81-3-5841-3410. Fax: 81-3-5841-3374. E-mail: seii@m.u-tokyo.ac.jp.

▽ Published ahead of print on 16 May 2007.

licate well only in the alimentary tracts of humans without showing neuropathogenicity, enough to elicit neutralizing antibodies against PV after oral administration.

Picornaviruses are sensitive to IFNs (3, 5, 24, 28, 46). IFNs play an essential role in the innate immune antiviral response. Recently, Ida-Hosonuma et al. (13) found that deletion of the IFN-α/β receptor (IFNAR) gene in hPVR-Tg (hPVR-Tg/*Ifnar*KO) resulted in the disruption of IFN-α/β signaling (27), which is an important determinant of the tissue tropism and pathogenicity of PV. Similarly, it has been reported that IFN-α/β plays an important role in the pathogenicity and tissue tropism of some viruses, including coxsackievirus and Theiler's virus in the *Picornaviridae* (6, 8, 26, 36, 42). These results suggest that not only hPVR (cell susceptibility) but also IFN-α/β (cell permissivity) contributes to the pathogenicity and tissue tropism of PV.

In this paper, we have clarified the instability of the virus in the gastric environment, where the low pH of the gastric contents inactivates PV. Furthermore, using hPVR-Tg with or without IFNAR expression, we have shown that IFN-α/β plays a key role in preventing PV from replicating in the intestines of mice.

MATERIALS AND METHODS

Viruses and cells. The virulent Mahoney strain [PV1(M)OM] and the avirulent Sabin 1 strain [PV1(Sab)IC-0] of type 1 PV derived from infectious cDNA clones pOM1 (41) and pVS(1)IC-0(T) (19), respectively, were employed in this study. As other virulent strains, Lansing (type 2) and Leon (type 3) were used.

African green monkey kidney (AGMK) cells were grown in Dulbecco's modified Eagle's medium (DMEM) supplemented with 5% newborn calf serum and were used for the preparation of viruses, transfection with infectious cDNA clones, and plaque assays.

Tg. The Tg strains used in this paper have been described previously (13). In brief, mice of a transgenic strain, ICR-PVRTg21 (21, 22), were backcrossed with C57BL/6 mice, and homozygotes with the C57BL/6 background (C57BL/6-PVRTg21) were produced. In this report, strain C57BL/6-PVRTg21 is referred to as PVRTg21. A129 mice, deficient in the *Ifnar* gene (27), were backcrossed with C57BL/6 mice and then further crossed with PVRTg21 or MPVRTg25-61 (MPVRTg25) (43). MPVRTg25 express hPVR under the control of the mouse PVR homolog (MPH) (25) regulatory gene. *PVR*$^{+/+}$ *Ifnar*$^{-/-}$ mice were obtained by intercrossing these PVRTg21/*Ifnar*KO (13) or MPVRTg25/*Ifnar*KO. All mice used were free of specific pathogens and were 7 to 10 weeks old. Mice were treated according to the guidelines for the Care and Use of Laboratory Animals of The University of Tokyo.

Assay of PV inactivation. PV1(M)OM (5 μl) was incubated at 37°C or 0°C for the periods indicated with 45 μl of each solution, and then the titer of virus was determined by a plaque assay. The pH 1 solution was 0.1 N HCl, the pH 2 solution was 0.01 N HCl, the pH 3 solution was 0.001 N HCl, and the pH 7 solution was saline. The pH of each solution was measured using pH test paper at the start and end points of the incubation.

Administration of viruses. For sampling of the gastric contents, mice were fasted overnight and then anesthetized with an intraperitoneal injection of 300 to 400 μl of ketamine (10 mg/ml) and xylazine (0.2 mg/ml) in saline. The stomach was exposed, and the pylorus was ligated with silk thread. The mice were inoculated with 200 μl of saline by using a gastric tube, and the gastric contents were collected. The gastric contents were centrifuged at 15,000 rpm for 10 min, and the supernatant was filtered. The filtrate was used for the experiments.

The viruses were administered orally using quantitative water bottles (Drinko-Measurer DM-G1; O'Hara & Co., Ltd., Japan). First, mice were fasted overnight, and then 2 ml of a viral solution containing 3% $NaHCO_3$ per mouse was administered within 24 h using the water bottles. The time point for starting the administration was taken as time zero. Twenty-four hours after the administration was started, the quantitative water bottles were replaced with conventional water bottles.

Recovery of viruses from tissues. For determination of the titer of virus in the tissues, the mice inoculated with the viruses were anesthetized and whole blood was recovered from the right ventricle. Immediately, the mice were perfused with saline through the left ventricle, and the tissues were excised. The tissues were homogenized in DMEM without serum to prepare a 10% emulsion. The homogenates were centrifuged to remove any debris, and the supernatant containing the virus was subjected to a plaque assay.

Labeling of PV. PV was purified by a protocol described previously (16). HeLa S3 cells were infected with PV1(M)OM at a multiplicity of infection of 10. The cells were harvested at 7 h postinfection, and the virus was purified from cytoplasmic extracts of the infected cells by using DEAE-Sepharose CL-6B (GE Healthcare Bio-Sciences KK) followed by centrifugation on a sucrose density gradient and CsCl equilibrium centrifugation. Purified virus was desalted by gel filtration on a PD-10 column (GE Healthcare Bio-Sciences KK) equilibrated with phosphate-buffered saline [PBS(−)] (per liter, 8.00 g NaCl, 1.15 g Na_2HPO_4, 0.20 g KCl, 0.10 g $MgCl_2 \cdot 6H_2O$, 0.20 g KH_2PO_4 [pH 7.4]). The concentration of poliovirions was determined by measuring the absorbance at 260 nm, where 1.0 optical density unit is regarded as equivalent to 9.4×10^{12} virions. The labeling of the virus is based on a protocol kindly provided by Lucas Pelkmans (32). PV (0.4 mg at 0.4 mg/ml) was labeled with 0.39 μl of Alexa Fluor 555-succinimidyl ester (10 mg/ml in dimethyl sulfoxide) according to the manufacturer's instructions (Invitrogen). These fluorophores react exclusively with free amines, resulting in a stable carboxamide bond. Labeled virus was repurified with NAP5 columns (GE Healthcare Bio-Sciences KK), dialyzed against PBS(−), and stored at −80°C. The labeling ratio was 14 mol of dye per mol of virus, and the specific infectivity of labeled virus was not reduced.

Detection of fluorescently labeled virus. After the MPVRTg25/*Ifnar*KO were anesthetized as described above, the intestines were exposed. The small intestine was ligated with silk thread at two points. Labeled virus was injected into the small intestine between the knots of the thread. One hour later, the injected portion of the small intestine was excised and washed with saline. The small intestine was directly observed under a confocal laser scanning microscope (LSM510; Carl Zeiss MicroImaging GmbH). For preparation of fixed tissue sections, the small intestine was immediately frozen in OCT compound (Sakura Fine Technical Co., Ltd.). Tissue sections were prepared by using a Jung CM3000 cryostat (Leica Instruments GmbH), mounted on 3-aminopropyltriethoxysilane-coated slides (Matsunami Glass Industries, Ltd.), and dried. All the staining procedures were performed at room temperature. First, the specimens were fixed in PBS(−) containing 2% paraformaldehyde for 1 min and washed four times in PBS(−). After treatment with 1.5% normal goat serum in PBS(−) for 20 min, 1 μg/ml of fluorescein isothiocyanate-labeled *Ulex europaeus* agglutinin-1 (UEA-1) was applied, and the specimens were incubated for 15 min and then washed with PBS(−). Nucleic acids were stained with 50 nM SYTO59 (Invitrogen). The sections were mounted with 80% (vol/vol) glycerol in PBS(−) and analyzed with a confocal laser scanning microscope.

Neutralizing assay. PVRTg21 and PVRTg21/*Ifnar*KO were orally administered 3×10^8 PFU of Sabin 1 along with 3% $NaHCO_3$ within 37 h by using quantitative water bottles. As a positive control, PVRTg21/*Ifnar*KO were intravenously injected with 1×10^5 PFU of Sabin 1. Twenty-one days after the administration, whole blood was collected from each mouse and serum was prepared after centrifugation. After incubation of the serum at 45°C for 1 h, 100 PFU of Sabin 1 in 100 μl was mixed with 100 μl of serially diluted serum and incubated for 1 h at 37°C. The virus-serum mixture was subjected to a plaque assay. Neutralizing activity is expressed as the maximum denominator for the dilution that can neutralize 100 PFU of Sabin 1.

RESULTS

Mouse gastric contents can inactivate PV. hPVR-Tg are much less susceptible to orally administered PV than humans. To explain this, we examined the stability of the virus during its passage through the mouse stomach after oral administration of PV. First, we examined whether a mouse gastric solution can inactivate PV. Under anesthesia, the pylorus was ligated and 200 μl of saline was inoculated using a gastric tube. Right after the inoculation, the gastric contents were collected, and the supernatant obtained by centrifugation was used as a gastric solution. As shown in Fig. 1A, 2×10^5 PFU of PV1(M)OM was incubated at 37°C or 0°C for the times indicated with or without the gastric solution from Tg or non-Tg. When PV was incubated at 37°C with the gastric solution from Tg or non-Tg, the titer of the virus was apparently reduced, whereas PV incubated with saline at 37°C for 4 h or PV just after mixing with the gastric solution showed no reduction. These results

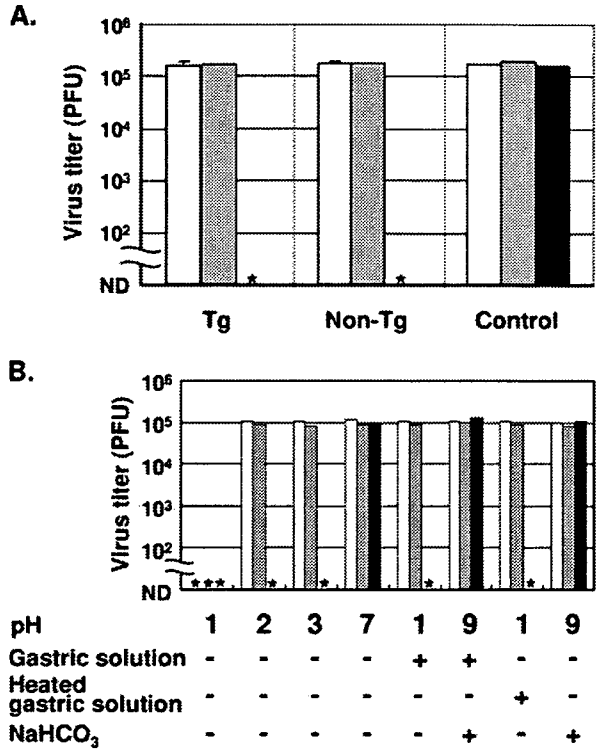

FIG. 1. Inactivation of PV with a mouse gastric solution. (A) PV1(M)OM at 2×10^5 PFU/5 μl was incubated at 37°C or 0°C for the periods indicated with or without 45 μl of a gastric solution from PVRTg21 (Tg) or C57BL/6 (non-Tg) mice, and then the titer of virus was determined by a plaque assay. As a control, PV was incubated with 45 μl of saline. Three animals were used per group. (B) PV1(M)OM at 1×10^5 PFU/5 μl was incubated at 37°C or 0°C for the periods indicated with 45 μl of each solution. After the incubation, the titer of virus was determined by a plaque assay. Open bars, samples just after mixing; solid bars, incubation at 37°C for 4 h; shaded bars, incubation at 0°C for 4 h. Asterisks, nondetectable titers. ND, not detected.

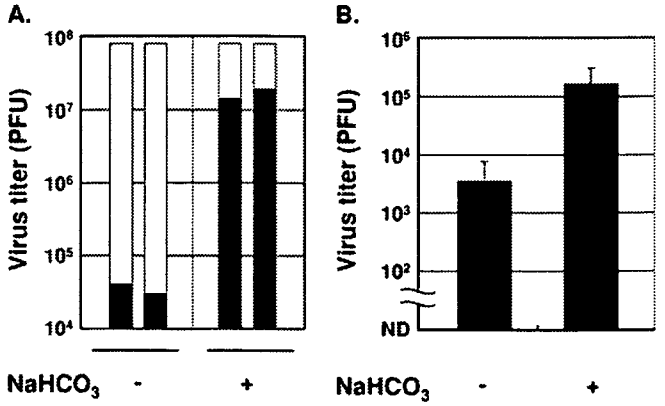

FIG. 2. Effect of passage through gastric contents on the virus titer after intragastric inoculation of mice with PV. (A) The effect of mouse gastric contents in the stomach on the retention of PV was examined. Under anesthesia, the pylorus was ligated and MPVRTg25 were intragastrically inoculated with 7.8×10^7 PFU of PV1(M)OM/500 μl with or without 3% $NaHCO_3$ by using a gastric tube. Five minutes after inoculation, the gastric contents were quickly recovered and the virus was detected by a plaque assay. Each bar represents an individual mouse. The black area indicates the titer detected in the gastric contents, and the white area indicates the decrease in the inoculated titer. (B) The rate of recovery of the virus from the small intestines of MPVRTg25 was examined after intragastric inoculation with 7.8×10^7 PFU of PV1(M)OM/500 μl with or without 3% $NaHCO_3$. Four hours after the inoculation, the contents of the small intestinal lumen were recovered and the virus was detected by a plaque assay. ND, not detected.

suggest that the gastric solution inactivated PV at 37°C independently of hPVR expression in mice.

Next, we investigated which factor influenced the inactivation. To examine the effect of low pH, 1×10^5 PFU of PV1(M)OM was incubated either with an HCl-containing solution at pH 1, pH 2, or pH 3, with saline (pH 7), or with the gastric solution, with or without $NaHCO_3$, either unheated or heated to inactivate the enzymatic activities. The gastric solution had a pH of ~1 without supplementation and a pH of 9 after it was mixed with $NaHCO_3$. As shown in Fig. 1B, PV was inactivated by the pH 2 and pH 3 solutions, as well as by the gastric solution after incubation at 37°C, but not by saline (pH 7). With the pH 1 solution, PV was inactivated without incubation at 37°C or 0°C. These results suggest that a low pH can inactivate PV. To confirm the effect of the low pH, the gastric solution with $NaHCO_3$ was incubated with PV. The pH 9 gastric solution did not inactivate PV even after incubation at 37°C. As a control, a saline solution with $NaHCO_3$ (pH 9) was examined; it had no effect on the viral titer. These results suggest that the low pH of the gastric solution leads to inactivation of the virus. When HEPES was used instead of $NaHCO_3$ to bring the viral solution to a pH of 9, the titer of virus was not decreased, either (data not shown). This result further supports the dependence of the PV-inactivating effect on a low pH. Finally, our experiment aimed to determine whether gastric enzymatic activities affect the infectivity of the virus. The enzymatic activities in the gastric solution were eliminated by heating at 95°C for 5 min. The heated gastric solution inactivated the virus after incubation at 37°C similarly to the unheated gastric solution without $NaHCO_3$. This result suggests that the enzymatic activities in the gastric solution do not affect the infectivity of PV under the conditions used.

Efficient delivery of PV to the intestine after intragastric inoculation with a pH neutralizer. To examine the survival rate of the virus at a low pH in the gastric environment in vivo, an assay of infectious PV was conducted after the virus was incubated in the stomach (Fig. 2A). Under anesthesia, the pylori were ligated and the mice were intragastrically inoculated with 7.8×10^7 PFU of PV/500 μl with or without 3% $NaHCO_3$ by using a gastric tube. Five minutes after inoculation, the gastric contents were quickly recovered and the titer of the virus was determined by a plaque assay. When the mice were inoculated with PV without 3% $NaHCO_3$, the titer was less than 0.1% of the original amount inoculated. On the other hand, when the mice were inoculated with PV together with 3% $NaHCO_3$, around 20% of the inoculated virus was recovered from the stomach. These results suggest that PV can be inactivated by gastric contents in vivo similarly to the inactivation in vitro (Fig. 1). As shown in Fig. 1B, the virus with the gastric solution containing 3% $NaHCO_3$ exhibited no loss of titer, whereas the virus inoculated intragastrically with 3% $NaHCO_3$ showed an 80% loss of titer in vivo (Fig. 2A). The gastric solution used for the in vitro experiments had been diluted with saline, which may have resulted in the minor effect on the inactivation of PV.

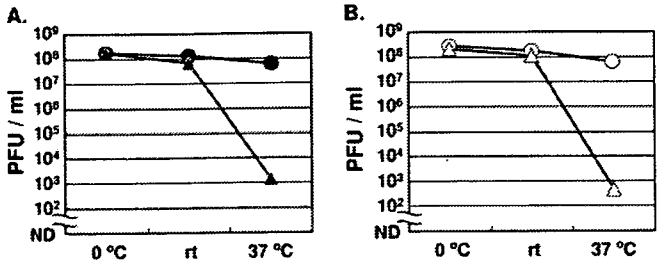

FIG. 3. PV titer after incubation for 24 h with or without $NaHCO_3$. A total of 1.5×10^8 PFU/ml of PV1(M)OM (A) or Sabin 1 (B) was incubated at the indicated temperatures for 24 h with (triangles) or without (circles) 3% $NaHCO_3$. The titer of virus after incubation was determined by a plaque assay. rt, room temperature. ND, not detected.

Next, we examined how much virus can reach the small intestine from the stomach after intragastric inoculation using a gastric tube. The rate of recovery of the virus from the small intestine was examined after intragastric inoculation of 7.8×10^7 PFU of PV with or without 3% $NaHCO_3$ by using a gastric tube. Four hours after inoculation, the contents of the entire small intestine were recovered and the titer of the virus was determined by a plaque assay (Fig. 2B). For mice inoculated with PV without 3% $NaHCO_3$, approximately 10^3 PFU/small intestinal lumen was recovered, whereas for mice inoculated with PV together with 3% $NaHCO_3$, about 10^5 PFU/small intestinal lumen was recovered. These results indicate that $NaHCO_3$ increased the recovery of the virus from the small intestinal lumen after intragastric inoculation with PV.

To know whether there is a reduction in the titer of the virus during the oral administration period (24 h), the stability of PV with 3% $NaHCO_3$ after 24 h was examined. The pH of a 3% $NaHCO_3$ solution was measured by pH test paper and determined to be 9. The titer was examined after incubation for 24 h at 0°C, room temperature, or 37°C (Fig. 3A and B). When PV1(M)OM was incubated with 3% $NaHCO_3$ or with H_2O, the titer did not decrease at 0°C or at room temperature. On the other hand, incubation of PV1(M)OM with 3% $NaHCO_3$ at 37°C reduced the titer by approximately 5 orders of magnitude, whereas incubation with H_2O at this temperature caused only about a 1-log-unit reduction (Fig. 3A). As for Sabin 1, when the virus was incubated at 0°C with 3% $NaHCO_3$ or with H_2O, no reduction in the titer was observed, whereas incubation at a higher temperature resulted in a reduction in the titer. Incubation of Sabin 1 with 3% $NaHCO_3$ or with H_2O at room temperature caused about a twofold reduction in the titer compared to that at 0°C. At 37°C, incubation of Sabin 1 with 3% $NaHCO_3$ reduced the titer by roughly 6 orders of magnitude, whereas incubation with H_2O caused only about a threefold reduction (Fig. 3B). These results suggest that incubation at room temperature for 24 h has only a minor effect on the titer and that incubation at 37°C for 24 h decreases the titer more severely, especially when the viral solution contains $NaHCO_3$. The relatively high pH of the 3% $NaHCO_3$ solution might have led to the instability of the viral RNA genome and virion particle. As for PV type 2 and 3 strains, incubation with 3% $NaHCO_3$ had only a minor effect on Leon, but Lansing showed a ~1-log-unit decrease in the titer after incubation with $NaHCO_3$ even at room temperature for 24 h (data not shown). These results suggest that the stability of PV with $NaHCO_3$ depends on the viral strain.

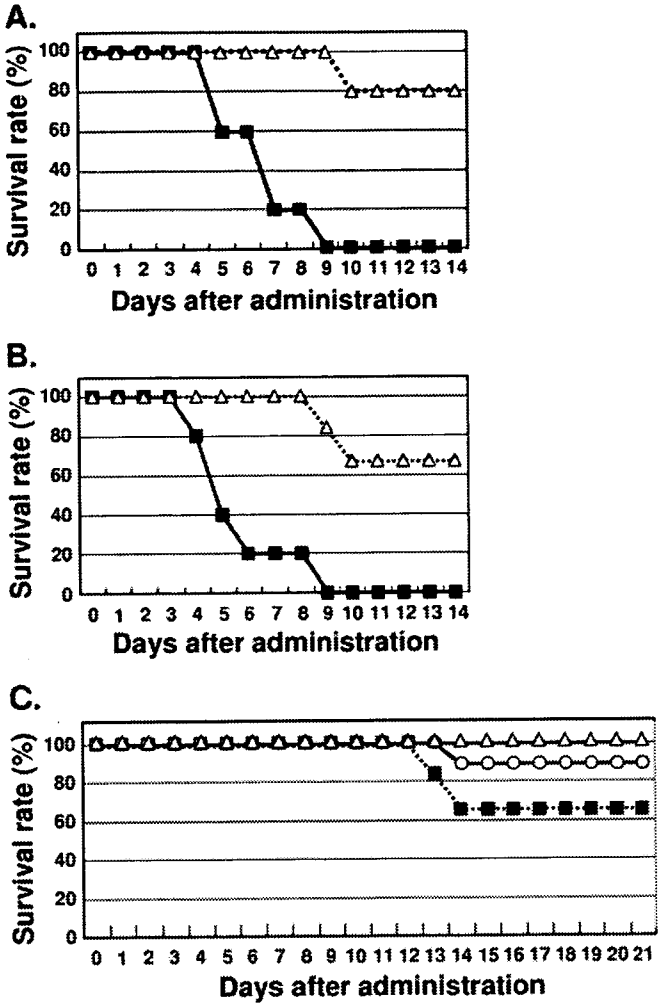

FIG. 4. Survival rates of mice after oral administration of PV. (A and C) PVRTg21/*Ifnar*KO (solid squares) or PVRTg21 (open triangles) were orally administered 3×10^8 PFU/2 ml of PV1(M)OM (A) or Sabin 1 (C), and the rate of survival was determined. Alternatively, PVRTg21/*Ifnar*KO were intravenously injected (open circles) with 1×10^5 PFU of Sabin 1/100 μl (C). Five (A), six (C) (oral administration), or nine (C) (intravenous injection) mice were observed for each group. (B) Similarly, MPVRTg25/*Ifnar*KO (solid squares) or MPVRTg25 (open triangles) were orally administered 3×10^8 PFU of PV1(M)OM/2 ml. Five or six mice were observed per group. The rate of survival was determined.

Effects of IFN-α/β signaling on the cell permissivity of orally ingested PV. To test whether PV orally ingested with 3% $NaHCO_3$ can cause paralysis in hPVR-Tg, PV with 3% $NaHCO_3$ was orally administered to PVRTg21 or to PVRTg21/*Ifnar*KO, which are deficient in *Ifnar*. To eliminate the possibility that the gastric tube might damage epithelia in the esophagus, 3×10^8 PFU of PV1(M)OM with 3% $NaHCO_3$ was orally administered without using a gastric tube. Eighty percent of PVRTg21 survived, whereas all the PVRTg21/*Ifnar*KO showed paralysis and died within 9 days of PV administration (Fig. 4A). These results suggest that PVRTg21/*Ifnar*KO are more susceptible to orally administered PV1(M)OM than PVRTg21. The susceptibility of

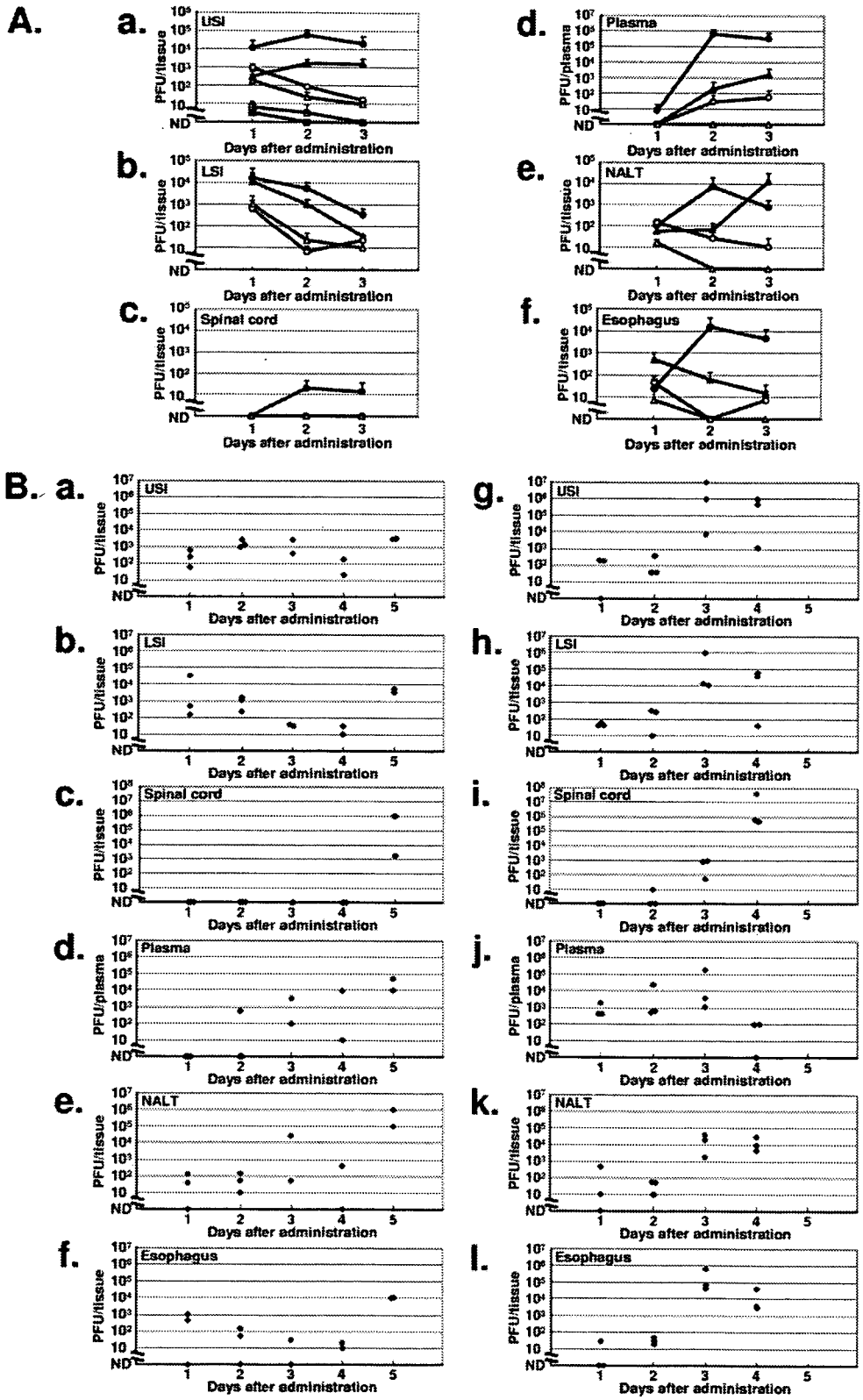

FIG. 5. Titers of PV recovered in tissues after oral administration of PV. (A) Virus was extracted from tissues of mice (PVRTg21 [open triangles], PVRTg21/*Ifnar*KO [solid triangles], MPVRTg25 [open circles], MPVRTg25/*Ifnar*KO [solid circles], C57BL/6 [open squares], and C57BL/6/*Ifnar*KO [solid squares]) 1, 2, and 3 days after the administration of 3×10^8 PFU of PV1(M)OM/2 ml. The vertical axis shows the amount (PFU) of PV detected in tissues by the plaque assay. USI, upper small intestine; LSI, lower small intestine. (B) Virus was extracted from each tissue of PVRTg21/*Ifnar*KO every 24 h after oral administration of 3×10^8 PFU of PV1(M)OM/2 ml (a to f) or intravenous injection of 1×10^5 PFU of PV1(M)OM/100 μl (g to l). Each point indicates one mouse. ND, not detected.

PVRTg21/*Ifnar*KO is dependent on the titer of virus (data not shown).

To confirm the effect of IFN signaling on the pathogenicity of orally administered PV in mice, another Tg strain (MPVRTg25) was examined, because hPVR is apparently detected in the small intestine and liver of MPVRTg25 by Western blotting (43). MPVRTg25 and MPVRTg25/*Ifnar*KO were orally administered PV with 3% $NaHCO_3$ without using a gastric tube, and the clinical symptoms were observed (Fig. 4B). In agreement with the results obtained with PVRTg21 and PVRTg21/*Ifnar*KO, all the MPVRTg25/*Ifnar*KO died whereas only 33% of MPVRTg25 died. These results suggest that MPVRTg25/*Ifnar*KO are more susceptible to oral administration of PV than MPVRTg25. These findings further support the notion that IFN signaling contributes to cell permissivity in mice orally administered PV. As for the clinical symptoms, MPVRTg25/*Ifnar*KO tend to show hepatocirrhosis rather than paralysis, and it is highly possible that these mice died of a hepatic disorder. Nevertheless, one can observe paralysis after intracerebral inoculation of MPVRTg25/*Ifnar*KO (data not shown). This result suggests that the virus can replicate in the CNS and cause paralysis even in MPVRTg25/*Ifnar*KO.

When PVRTg21/*Ifnar*KO or PVRTg21 were orally administered Sabin 1 with 3% $NaHCO_3$ without use of a gastric tube, more than 30% of PVRTg21/*Ifnar*KO showed paralysis and died, whereas all the PVRTg21 survived for 21 days (Fig. 4C). These results suggest that PVRTg21/*Ifnar*KO were more susceptible to oral administration of Sabin 1 than PVRTg21. PVRTg21/*Ifnar*KO also showed susceptibility to the type 2 strain Lansing or the type 3 strain Leon despite the fact that that Lansing was less pathogenic than PV1(M)OM or Leon (data not shown). Together with these results, our study strongly suggested that IFN signaling plays a key role in cell permissivity following oral administration of PV, although we cannot exclude the possibility that components of the innate immune system other than IFN-α/β affect the cell permissivity.

Time course of the replication of PV in tissues after oral administration. To assess the ability of PV to replicate in different tissues after oral administration, the titers of the virus in the small intestine, colon, nasopharynx-associated lymphoid tissue (NALT), esophagus, spinal cord, and plasma were determined at 1, 2, and 3 days after administration to mice. PV was orally administered to PVRTg21, PVRTg21/*Ifnar*KO, MPVRTg25, MPVRTg25/*Ifnar*KO, C57BL/6, and C57BL/6/*Ifnar*KO, and the tissues were excised each day after administration. The tissues were then homogenized, and the titers of the virus in the solutions were determined by a plaque assay (Fig. 5A). In all the tissues tested, titers were always higher in *Ifnar* knockout hPVR-Tg than in *Ifnar*-expressing hPVR-Tg. For instance, the titers were higher in PVRTg21/*Ifnar*KO than in PVRTg21, and similarly, they were higher in MPVRTg25/*Ifnar*KO than in MPVRTg25 (Fig. 5Aa to c, e, and f). As for C57BL/6/*Ifnar*KO and C57BL/6 mice, the titers in the upper small intestine were negligible (Fig. 5Aa). These results suggest that PV can replicate in all of the tissues examined more efficiently in *Ifnar* knockout mice than in *Ifnar*-expressing mice.

As for plasma, the virus caused viremia from the second day in PVRTg21/*Ifnar*KO, MPVRTg25, and MPVRTg25/*Ifnar*KO (except for one animal that showed slight viremia on the first day) (Fig. 5Ad). The results imply that the virus leaks into the blood after replicating in tissues, probably the alimentary tract, because little virus was detected in plasma on the first day.

We next investigated the chronological titer of the virus in different tissues after an oral or systemic challenge (Fig. 5B). When PVRTg21/*Ifnar*KO were intravenously inoculated with PV1(M)OM, the virus had started replicating extensively in all tissues examined on the third day (Fig. 5Bg to l). Almost all the mice injected intravenously with the virus developed paralysis and died on the fifth day (data not shown). Following oral administration of PV1(M)OM to PVRTg21/*Ifnar*KO, all the tissues examined showed a burst of proliferation of the virus on the fifth day (Fig. 5Ba to f), and the mice began to die on the fifth day (Fig. 4A). These findings indicate that the burst of replication after oral administration may be due to the virus that appeared on the second day in the bloodstream, because such a burst took 3 days after the intravenous injection. It seems feasible that the paralysis after oral administration of the virus is mainly due to the circulating virus that invaded from the alimentary tract.

Inoculated PV was incorporated into mouse small intestinal epithelia. To examine which kind of cells in the alimentary tract incorporate the virus, fluorescently labeled PV was injected into the ligated small intestine in MPVRTg25/*Ifnar*KO. One hour after the injection, the ligated tissue was subjected to confocal laser scanning microscopic analysis. As shown in Fig. 6Ab and c, the virus was detected inside the microvillus, whereas no fluorescence was detected in the small intestine without the injection (Fig. 6Ae and f). When the intestine was observed after frozen sectioning, the virus was detected in the cytoplasm of the epithelial cells in the microvilli (Fig. 6Bd and e). No fluorescence was detected in the small intestine without injection of the virus (Fig. 6Bi and j). These results suggest that the virus inside the cavity of the small intestine can be incorporated into the epithelial cells. It is highly possible that the incorporated virus starts to replicate in these epithelial cells. To further clarify which kinds of cells incorporate the virus from the intestinal cavity, fluorescently labeled UEA-1 (specific for α-L-fucose residues) was used, since UEA-1 has been shown to possess high affinity for selected intestinal epithelial cells, including mouse microfold (M) cells and goblet cells (4, 17). As shown in Fig. 6C, PV was not detected in the UEA-1-positive fraction of epithelial cells. On the other hand, the cells that contained PV were the UEA-1-negative fraction in the epithelia (Fig. 6B). It has been reported that some microorganisms, such as *Salmonella enterica* serovar Typhimurium and *Yersinia pseudotuberculosis*, can be efficiently incorporated into M cells under similar experimental conditions (15). These results suggest that in the IFN-α/β-free environment of the intestinal epithelium, PV is incorporated into the UEA-1-negative fraction of epithelial cells, although we cannot exclude the possibility that M cells are involved in the dissemination of the virus and the subsequent infection process.

Oral administration of attenuated PV did not effectively generate neutralizing antibodies in hPVR-Tg/*Ifnar*KO. Inasmuch as orally administered PV is incorporated into the intestinal epithelium and starts replicating in hPVR-Tg/*Ifnar*KO, it is important to examine whether oral administration of attenuated PV can induce the production of neutralizing antibodies in mice. To this end, attenuated PV was orally administered to

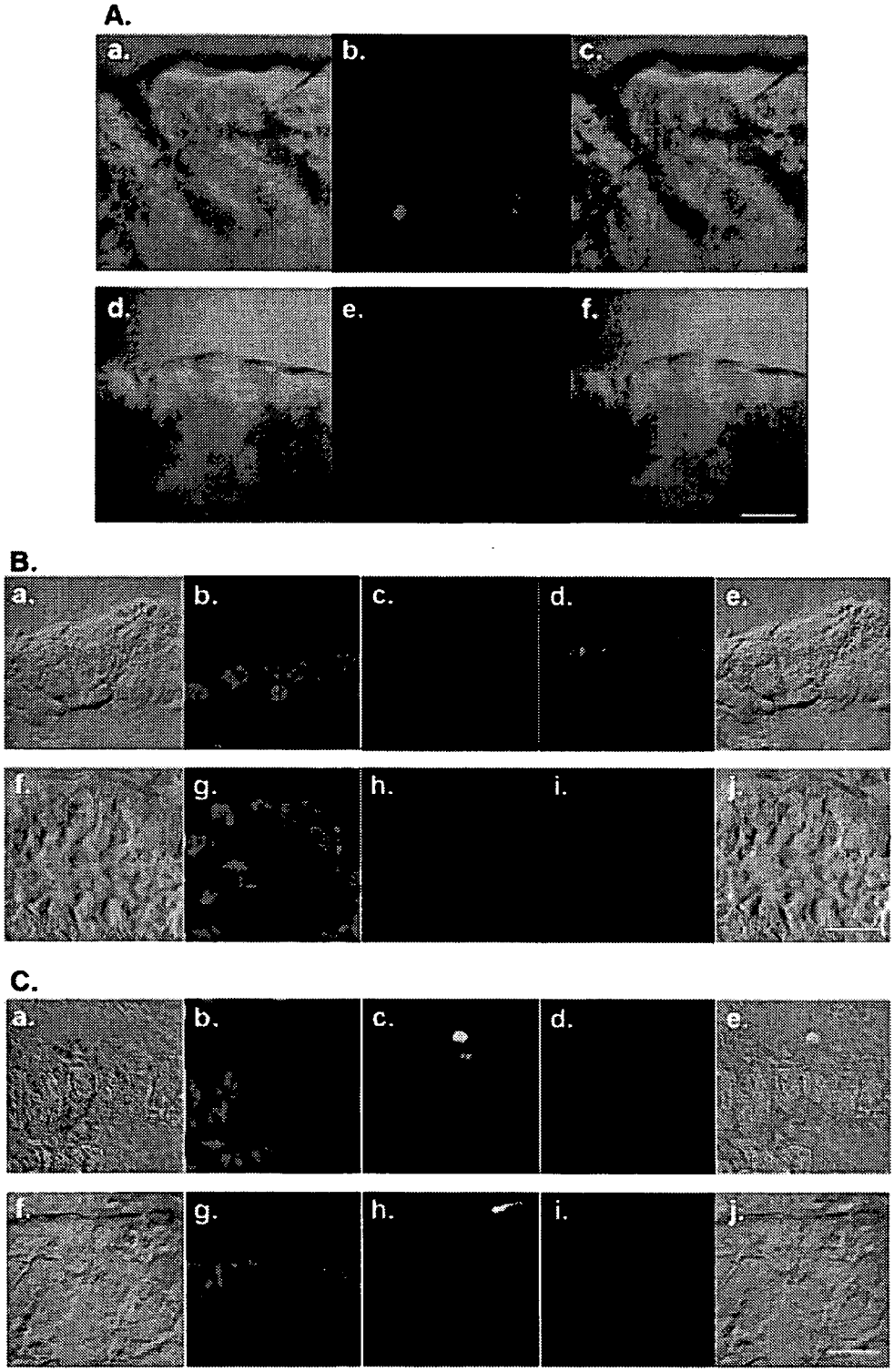

FIG. 6. Fluorescently labeled PV is detected in intestinal epithelia. Alexa Fluor 555-labeled PV1(M)OM (1.5×10^7 PFU/10 μl) was injected into the ligated small intestines of MPVRTg25/*Ifnar*KO (top row of images in each panel). PV-negative controls were also used (bottom row in each panel). One hour after injection, the ligated portion was excised and subjected to confocal laser scanning microscopy. Intestines were observed without (A) or with (B and C) fixation and frozen sectioning. (B) UEA-1-negative epithelia; (C) epithelia that contain UEA-1-positive cells. Red, Alexa Fluor 555-labeled PV1(M)OM (Ab, c, e, and f; Bd, e, i, and j; Cd, e, i, and j); blue, nuclei (Bb, e, g, and j; Cb, e, g, and j); green, fluorescein isothiocyanate-labeled UEA-1 (Bc, e, h, and j; Cc, e, h, and j). Aa and d, Ba and f, and Ca and f show bright-field images only. Ac and f, Be and j, and Ce and j show merged images of bright-field and fluorescence micrographs. Bars, 100 μm.

TABLE 1. PV-neutralizing activity in serum after oral administration of Sabin 1

Mouse strain	Substance	Route of administration	Amt of immunizing virus (PFU/mouse)	Neutralizing activity[a]
PVRTg21/*Ifnar*KO	DMEM	Oral	0	0/6
	Sabin 1	Oral	3×10^8	0/4
	Sabin 1	Intravenous	1×10^5	8/8
PVRTg21	Sabin 1	Oral	3×10^8	0/6

[a] Expressed as the number of mice whose serum showed neutralizing activity (≥16)/number of mice examined.

PVRTg21/*Ifnar*KO or PVRTg21. Serum was collected 21 days after virus administration, and the neutralizing activity in the serum was assayed. In the case of PVRTg21/*Ifnar*KO, all the mice showed neutralizing activity after intravenous inoculation of 10^5 PFU of Sabin 1 whereas no mouse showed neutralizing activity after oral administration of 3×10^8 PFU of the strain or DMEM (Table 1), although the virus was detected in the intestine until 4 days after oral administration of Sabin 1 (data not shown). As for PVRTg21, no mouse showed neutralizing activity after oral administration of 3×10^8 PFU of Sabin 1. Similar results were obtained for MPVRTg25/*Ifnar*KO after oral administration of the strain (data not shown). These results suggest that oral administration of Sabin 1 to PVRTg21/*Ifnar*KO or MPVRTg25/*Ifnar*KO was ineffective at raising the neutralizing activity.

DISCUSSION

Some of the recent outbreaks in areas certified as being clear of polio were caused by a circulating vaccine-derived PV that had mutated from the oral polio vaccine used to prevent polio (18). This suggests to us a need to develop new polio vaccines or antipolio drugs for the control of polio outbreaks. For that purpose, it is necessary to establish a useful animal model that mimics the natural infection route and subsequent disease development in humans in order to evaluate candidate vaccines or drugs.

A paper about the effects of pH on PV infectivity (40) indicates that PV can be easily inactivated at pH 3.0 or 9.0 at 30°C, but it depends on the buffers. This means that, at least at pH 3.0 or 9.0, the stability of viral infectivity is determined by the stability of the virions in particular buffers.

There is a discrepancy in the data obtained at pH 1 between the HCl solution and the gastric solution (Fig. 1B). The fact that the pH was measured using pH test paper and we cannot know the value precisely might explain the discrepancy, especially at the extremely low pH.

The present study has shown that IFNAR plays an important role in the infection and multiplication of orally administered PV in the small intestine of hPVR-Tg (Fig. 4 and 5A). The deletion of IFNAR resulted in successful infection by oral PV via the intestinal epithelium and the subsequent development of clinical symptoms. Viremia seems to be essential for the symptoms to appear (Fig. 5B), and a histopathology for similar symptoms caused by artificial viremia (intravenous inoculation) in hPVR-Tg/*Ifnar*KO has been reported (13). We thus established an oral administration system using hPVR-Tg/*Ifnar*KO, with which one can assess the 100% lethal doses of PV strains. This is the first in vivo system in which all the animals showed paralysis after oral administration of PV.

From the results presented in Fig. 5B, the orally administered virus disseminates mainly through the bloodstream in mice, although other, minor routes might be involved. It is possible, for example, that a neural pathway exists from the alimentary tract to the CNS through the vagus nerve or from the skeletal muscle to the CNS through the peripheral nerve. After PVRTg21/*Ifnar*KO were orally administered 3×10^8 PFU of Sabin 1, low titers (from 4×10^1 PFU/plasma to 8×10^2 PFU/plasma) of virus were detected in the plasma for 2 of 3 mice 3 days after administration and for 1 of 3 mice 4 days after administration. In spite of the ineffective serum conversion (Table 1), some lethal infection occurs after oral administration of Sabin 1 in PVRTg21/*Ifnar*KO (Fig. 4C). These results imply that the neural pathway from the alimentary tract to the CNS might contribute to death after oral administration of Sabin 1 in PVRTg21/*Ifnar*KO. After oral administration, the titer of virus in skeletal muscle did not rise until the virus started replicating efficiently in all the tissues examined (data not shown). This result implies that the neural pathway from skeletal muscle to the CNS is not essential, at least in this system. Nevertheless, we do not know which pathway has an essential role in causing paralysis and death.

It is possible that the virus was incorporated accidentally via the intranasal pathway after oral administration. In our experiments, when 1.5×10^8 PFU/ml of the Mahoney strain was orally administered to PVRTg21, the mice showed hardly any signs of paralysis. This concentration was higher than 10^6 PFU/20 μl, which was enough to cause death among 60% of intranasally inoculated PVRTg21 (29). Furthermore, the distribution of the virus after oral administration differs from that after intranasal inoculation. From these results, it is unlikely that orally administered virus enters the intranasal pathway.

We have shown previously that hPVR is expressed in the small intestines of MPVRTg25 but is not detected in those of PVRTg21 by Western blotting (43). As for immunohistochemistry, hPVR expression was barely observed in the intestinal epithelium and was not detected in germinal centers within Peyer's patches in PVRTg21 (14), and an assertive hPVR antigen was not detected in small intestinal epithelia in PVRTg21 or MPVRTg25 (M. Takano-Maruyama and H. Ohno, personal communication). These results suggest that hPVR is not expressed at high levels in the small intestines of PVRTg21, MPVRTg25, or the *Ifnar* knockout versions of these mice, although it is possible that the levels of hPVR expression on the intestinal epithelia differ among these mice. Incorporated fluorescently labeled virus was observed in the intestines of MPVRTg25/*Ifnar*KO but not PVRTg21/*Ifnar*KO or C57BL/6 mice (data not shown). This might be due to the level of hPVR expression on the apical side of the intestinal epithelia. Despite the fact that PVRTg21 express little if any hPVR in the small intestine, the titers of virus in the upper small intestines of PVRTg21 and PVRTg21/*Ifnar*KO 1 day after administration were ~10^2-fold higher than those in C57BL/6 mice and C57BL/6/*Ifnar*KO, respectively (Fig. 5A), and PVRTg21/*Ifnar*KO showed susceptibility to oral administration of PV (Fig. 4A and C and 5). These results suggest that hPVR ex-

pressed in the small intestines of PVRTg21/*Ifnar*KO contributes to cell susceptibility to orally administered PV.

We observed hepatocirrhosis in MPVRTg25/*Ifnar*KO after oral administration of PV1(M)OM despite the fact that MPVRTg25 do not show hepatocirrhosis. These results suggest that MPVRTg25/*Ifnar*KO show irregular tissue tropism of the virus compared to MPVRTg25, which have a native immune system. A previous paper has reported that viral antigen-positive cells were detected in the liver 1 day after intravenous inoculation of 2×10^7 PFU of PV1(M)OM into MPVRTg25/*Ifnar*KO (13). Moreover, a high titer of the virus was recovered 2 days after oral administration of 3×10^8 PFU of PV1(M)OM to MPVRTg25/*Ifnar*KO (data not shown). It seems that this occurred because hPVR in the liver causes the virus to replicate in MPVRTg25/*Ifnar*KO mice. Indeed, we have reported previously that the liver in MPVRTg25 expresses hPVR (43). Moreover, the virus in the bloodstream can easily access the liver (1). Considering these results, it is feasible that the viremia led to a liver infection that then caused a secondary viremia, leading to invasion of the CNS in MPVRTg25/*Ifnar*KO. As for PVRTg21/*Ifnar*KO, it has been reported that the disruption of IFNAR enables the virus to replicate in nonneuronal tissues, although both PVRTg21 and PVRTg21/*Ifnar*KO developed paralysis by similar points in time after intravenous inoculation (13). All together, the oral infection system using hPVR-Tg/*Ifnar*KO does not serve as an adequate animal model for analyzing virus tissue tropism in the whole body, although the clinical symptoms seen in PVRTg21/*Ifnar*KO were similar to those in PVRTg21. This notion is also supported by the fact that healthy humans are highly susceptible to poliovirus infection in spite of a robust innate immune response. Nevertheless, this oral administration system might be applicable to the study of initial infection events in vivo. It is also worth elucidating the role of the IFNAR-related signaling cascade in the infection of intestinal epithelial cells.

We succeeded in detecting the fluorescently labeled virus in the small intestine 1 h after its injection (Fig. 6) but failed to detect the viral antigen 2 days after oral administration of the virus using immunohistochemistry (data not shown). It is difficult to detect antigens in the intestine because of high background levels and the quick turnover of infected cells. It is possible that the virus does not replicate prominently in the intestinal epithelia or that the infected cells tend to drop out easily from the epithelial layer. Although the titers of virus in other alimentary tissues were relatively low after oral administration of the virus (Fig. 5A) and the viral antigen was not detected in the NALT, esophagus, or colon 2 days after oral administration (data not shown), we cannot exclude the possibility that PV replicates in the alimentary tract early in the course of infection. Alternatively, the fluorescence observed could have derived from inactive PV taken up by cells during a nonproductive infection.

The mechanism for oral infection with PV in humans has not been made clear, though it is possible that PV can replicate in and/or permeate M cells or lymphatic tissues in humans, because attenuated PV vaccine strains can readily generate neutralizing antibodies. In the present study, oral administration of Sabin 1 did not lead to the generation of neutralizing activity in the serum of PVRTg21/*Ifnar*KO (Table 1) and MPVRTg25/*Ifnar*KO (data not shown) or the binding activity of immunoglobulin A's in feces (data not shown), despite the fact that the virus proliferated in the upper small intestine (data not shown). Our results also showed that PV was not preferentially detected in the UEA-1 fraction of epithelial cells, which contains M cells, in hPVR-Tg/*Ifnar*KO (Fig. 6C), and the virus did not proliferate efficiently in NALT, a lymphatic tissue (Fig. 5Ae and Be). These results may correlate with the difficulty of raising the neutralizing activity after oral administration of the virus in hPVR-Tg/*Ifnar*KO. However, it should be emphasized that a lack of IFNAR hampered enhancement of the antibody-evoked response (23). Thus, the phenomena we observed might be due to the lack of IFNAR. Although we still could not reconcile the discrepancy between humans and the murine model in the exact site of PV invasion in the intestinal tract, the present study offers a new opportunity to address the issue, since hPVR-Tg/*Ifnar*KO are susceptible to orally administered PV for the initiation of infection and subsequent development of disease symptoms. And it is probable that the expression of hPVR in different intestinal cells is important in determining the heightened permissiveness of oral PV administration in humans compared to rodents. PV is highly successful at infection of the alimentary tracts of humans, and intestinal secretion of the virus can persist for months, even in healthy individuals, regardless of age. This means that the virus infects and replicates in some cells or tissues in the human gastrointestinal tract in spite of a possible early innate immune response. However, it is also possible that the innate immune response of humans is weaker than that of rodents.

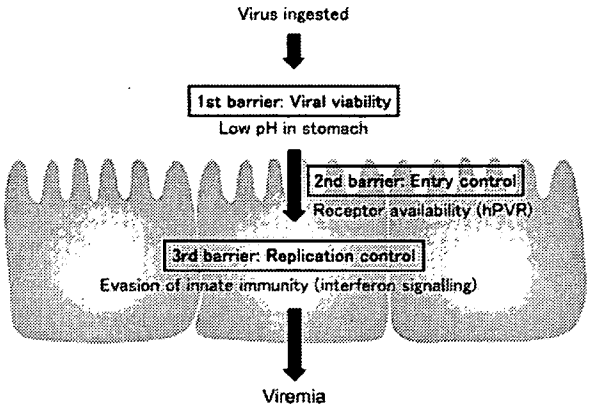

FIG. 7. Presumed PV dissemination routes and characteristics. The presumed barriers to orally ingested PV are shown. First, the ingested virus enters the stomach and suffers a low-pH environment (the first barrier). Second, the virus has to find the appropriate receptor in order to enter the intestinal cells (the second barrier, cell susceptibility). Third, the virus can start replicating in the cells depending on the lack of an IFN system (the third barrier, cell permissivity). Finally, the virus probably invades the bloodstream.

The presumed barriers to orally ingested PV are shown in Fig. 7. First, the ingested virus enters the stomach and experiences a low-pH environment (the first barrier). If the virus overcomes this, it has to find the appropriate receptor in order to enter the intestinal cells (the second barrier, cell susceptibility). Then the virus can start replicating in the cells depending on the lack of an IFN system (the third barrier, cell permissivity). Finally, the virus probably invades the bloodstream. In this report, we clarified that the low pH of the gastric